Textile Electronics for VR/AR Applications

Su Liu[1], Kitming Ma[1], Bao Yang[1], Heng Li[1,2] and Xiaoming Tao[1]*
[1]Research Center for Smart Wearable Technology
Institute of Textiles and Clothing
[2]Department of Building and Real Estate
Hong Kong Polytechnic University, Hong Kong, China
Xiao-ming.tao@polyu.edu.hk

Abstract

Textile electronics addresses fibers or fiber assemblies with electronic functions to generate, transmit, modulate, and detect electrons. Interactive textile electronic devices may provide suitable platforms for virtual reality (VR) / augmented reality (AR) applications because of their excellent performance and unique immersive features such as light-weight, handiness, flexibility, comfort, and low strain even under high deformations. This paper presents a systematic review of the literature on the state-of-the-art of interactive devices, fabrication technologies, system integration, promising applications, and challenges involved in textile-based VR/AR systems.

Keywords: Textile electronics; Virtual reality; Augmented reality; Interactive devices.

1. Introduction

The term virtual reality was first introduced by Jaron Lanier in the 1980s.[1] Presently, VR is commonly conceptualized as a technical and scientific field that employs behavioral interfaces and computer science to simulate the behavior of three-dimensional (3D) objects in a virtual environment. Further, it allows one or more users to immerse and interact with each other in real-time through sensorimotor channels.[2] In 1997, Ronalad Azuma proposed a now commonly employed concept of augmented reality (AR) with three features: the combination of a physical world and virtual world, interaction in real-time, and registered in 3D.[3] VR/AR is a multidisciplinary technology that integrates computer, sensor, graphic image, communication, measurement and control multimedia, artificial intelligence, and other technologies. It ensures several key properties such as immersion, interaction, imagination, and augmentation. With the development of related technologies, VR/AR technologies are becoming increasingly sophisticated and present new experiences to human beings. The applications have expanded from military and aviation fields to many civilian fields such as education, architectural design, product design, visualization of scientific computing, remote services, and entertainment.[4]

Human beings are central to the VR and AR systems because virtual and augmented applications are purposed for people.[2] Mimicking human sensory and muscular/skeleton systems has been a major challenge in textile electronics. To date, audial and visual means have been widely developed for most VR/AR devices. However, if devices are bulky and stationary, the general public is less likely to wear such conspicuous devices as robotic exoskeletons.[5] Hence, textiles are a suitable platform for VR/AR applications owing to their excellent performance and unique features such as light-weight, handiness, flexibility, comfort, and low strain even under high deformation conditions.[6]

Textile electronics addresses fibers or fiber assemblies with electronic functions to generate, transmit, modulate, and detect electrons. They may have characteristic

functions in life intelligence, such as sensing, actuating, communicating, and learning, that are achieved either by building nanostructures on/within fibers or integrating microelectronic components into different textile structures.[7] In the past twenty years, textile electronic devices have started sensing surface bio-potentials, pressure, friction, strain, temperature, sweat, etc., to connect electronic devices and harvest energy to power wearable microelectronic systems. They have been employed in various VR applications such as social media, games, personal engagement, and entertainment.[8] **Figure 1** shows several types of textile electronics and their multifunctional applications in VR/AR, such as energy harvesting for supplying power, biopotential signals for monitoring human mental health and human−machine interface, human motion tracking, thermal haptic devices for microclimate control, actuators for providing tactile feedback, and textile displays for brain-interfaced communications.

Although textile electronics have been explored and reported in the last twenty years, the application of textile-based VR/AR systems is still in the initial stage. Thus, a systematic review of the development of sensory interactive devices, fabrication technologies, system integration, and promising applications of textile-based VR/AR systems is required.

In this review, we address the state-of-the-art textile-based VR/AR devices, systems, and applications. We first introduce the textile electronics including their definition, classification, fabrication technology, and system architecture in Section 2. In Section 3, interactive textile devices used in the VR/AR system are discussed. Then, we present various fabrication processes and examine certain VR/AR systems integrated with interactive textile devices, electronic interfaces, power supplies, and display hardware in section 4 and 5.

2. Textile Electronics

Textile is described as a second skin because it is in direct contact with the human body, thus providing a unique platform for the various functionalities of electronics, i.e., to generate, transmit, modulate, and detect electrons. Therefore, textile electronics can potentially become a new group of components for Internet of Things (IoT), VR/AR, and robotics applications. Textile electronic devices are lightweight, flexible, conformable, and breathable; they also possess electronic functionality and can interact with wireless networks. The development of textile electronics unlocks new avenues for the application of textile electronics, particularly for VR/AR. The primary focus of VR/AR is the interaction between virtual information, external world, and users.[9] To ensure social acceptance of VR/AR technology, the interaction between users and the interface must be simple, natural, intuitive behavior, and not distract users; also, the wearable devices should be compact. This section briefly introduces the materials and development of textile electronics and discusses their potential in VR/AR applications.

2.1 Intrinsic conductive fibers, yarns, and fabrics

As conductive materials are the basis of electronics, they should first be transformed from their conventional and rigid form to fibrous structures in a hierarchical approach (fiber-yarn-fabric-product). The materials can be consolidated into three groups: metals, intrinsically conductive polymers (ICPs), and carbon-based materials, such as graphene or carbon nanotubes.

Metal was among the first conductive materials used to develop flexible electronics because of its abundance and excellent electrical conductivity. For instance, the electrical conductivity of silver is approximately 6.30×10^7 S/m, [10] which is useful for

the functionalities of electronics. In the early stages of developing flexible electronics, many researchers developed conductive fibers or filaments via drawing or shaving techniques from metals such as copper, stainless steel, silver, brass nickel, and their alloys. The diameter of the metal fiber/filament can be achieved to 1−80 μm.[11] Dias et al. adopted multi-strand copper wires to connect electronic components and placed a carrier yarn parallel to the copper wire (**Figure 2a**). The flexible yarn thus produced could be integrated with LED chips and exhibited a strength of 98 N.[12] However, the variation in stiffness, brittleness, and weight of the metallic fiber or yarn limits its applications; metallic fibers or filaments are generally blended with other commercial fibers to improve their textile properties. For example, copper and stainless steel wires are spun with cotton to produce conductive yarn by ring spinning.[13] However, because the modified metallic yarn deviates from commercial textile materials, recent research on metallic materials has focused on coating techniques at the nanoscale, such as nanowires[14] and nanorods, where the textile substrate acts as the base. Because of their thinner diameter and high aspect ratio, nanostructures act as basic building blocks for optoelectronic, sensor, and other applications.[15] Nanowires are 1D nanostructures with diameters in the range of 10−200 nm and lengths in the range of 5−100 μm. The resistivity of Ag nanowire-fiber is lower to 0.8 Ω/cm.[16] In 2012, Xu et al. developed highly conductive and stretchable Ag nanowires (AgNWs) by drop-casting suspension AgNWs on a silicon wafer (**Figure 2b**).[17] AgNW films of varied thicknesses were obtained after drying. Subsequently, liquid polydimethylsiloxane (PDMS) was poured on the AgNW film. After the PDMS was cured and substrate was peeled off, the AgNW film penetrated the top surface of the cured PDMS. The resulting AgNW-based conductors exhibited a superior conductivity of 5285 S/cm even after several stretching/releasing tests in the tensile strain range of approximately 50%.[17] In 2012, Lee et al. fabricated long AgNWs and employed them as a metal electrode.[18] The length of the AgNWs was increased to more than 500 μm via a novel successive multistep growth method using repetitive $AgNO_3$ reduction in ethylene glycol solution with poly(vinyl pyrrolidone) (PVP).[18] The AgNWs demonstrated excellent transparency from 90% to 96% and high electrical conductivity in the range of 9−70 Ω/sq.[18] An et al. developed a supercapacitor based on vertically aligned gold nanowires (AuNWs).[19] The AuNWs were grown on a 100% pre-strain Ecoflex substrate. **Figure 2c** showed the schematic of the synthesized AuNW. However, metallic nanowires are rough and slightly unstable. Further investigations should be conducted for a better control over their morphologies and properties.[20]

Conductive polymers are intrinsically flexible and can be blended with other materials. The mechanism of conductivity is the formation of conjugated double bonds in the chemical structure and doping process to facilitate oxidation or reduction.[21] Most prominent conductive polymers are polyaniline (PANI), poly(3,4-ethylenedioxythiophene) polystyrene sulfonate (PEDOT:PSS), and polypyrrole (PPy). PANI has the advantages of lower production cost and superior thermal stability when compared to the other polymers.[21] Uh et al. adopted PANI to develop a conductive fiber with a conductivity of 20 S/cm (**Figure 2d)**.[22] PEDOT:PSS is widely adopted in different aspects of textile electronics because of its good thermal and environmental stability, conductivity, optical transmission, water solubility, and processability.[23] Wang et al. fabricated a highly stretchable and conductive film by incorporating ionic additives-assisted stretchability and electrical conductivity (STEC) enhancers into PEDOT:PSS **(Figure 2e)**.[24] After 1000 cycles and 100% strain, the resulting polymer film showed excellent conductivity at 3600 S/cm. Riquelme et al. improved the wet-spinning process to produce PEDOT: PSS fibers.[25] The diameter of the fibers was as

small as 6.7−7 μm and their conductivity was 2000 S/cm. Yuan et al. spun PEDOT: PSS fibers with 100 Ω/cm conductivity, which were utilized to produce supercapacitors (119 $mFcm^{-2}$).[26] However, PPy exhibits good biocompatibility and environmental stability. Číková et al. synthesized polycaprolactone/PPy fibers by electrospinning a solution mixed with PCL and pyrrole monomer.[27] After coating PPy **(Figure 2f)** on PCL fibers, the samples attained a conductivity of 1 S/cm. The conductivity of IOPs is mainly in the range of semiconductors,[21] which is the distance to metal conductivity. The common solution to improve conductivity of polymer is the addition of other conductive materials, such as graphene and carbon black, in the polymers.

Carbon-based materials are another prospective materials for textile electronics because they exhibit an appropriate tensile strength, electrical conductivity, and specific surface area. They constitute carbon nanotube fibers (CNTFs), carbon fibers, and graphene fibers.[28] The structures of single-walled carbon nanotubes (SWCNTs) and multiwalled carbon nanotubes (MWCNTs) are shown in **Figure 2h** and **Figure 2g**, respectively.[29] The two types of carbon nanotubes (CNTs) exhibit high aspect ratios. Carbon fiber contains approximately 92 wt% carbon and features superior performance. It is produced from the carbonization of precursor fibers.[30] A precursor fiber can be PANI and pitch fiber. Kil et al. synthesized a pitch-based carbon fiber **(Figure 2i)** in the temperature range of 400−1200 °C at a heating rate of 5 °C/min.[31] CNTFs are produced by wet spinning or direct spinning from CNT assemblies, such as CNT aerogels and CNT arrays.[32] CNTFs demonstrate an electrical conductivity of approximately 300 S/cm and a mechanical strength of 460 MPa.[33] To improve the fiber density and twist angle of the fiber, Zhang et al. spun strong CNTFs from a CNT array by integrating the post-spinning procedure with the as-spun CNTFS.[34] CNTFs can be spun into a yarn, which can be knitted and woven into fabrics. Zhao et al. spun CNTFs from a CNT array and spun them into a yarn that was used as a strain sensor to monitor cracks in a composite structure.[35] Graphene fibers are mainly manufactured via wet spinning, in which polymer solution are mixed with graphene. As the graphene fiber is not an intrinsic fiber produced via conventional methods, researchers have tried to develop other fibers. Dong et al. developed a novel method to produce graphene fibers from graphene oxide sheets based on a hydrothermal reaction using a glass pipeline.[36]

2.2 Textile actuators

Actuators can convert energy from physical domains into various motions in order to control and move objects to produce feedback or sensation. However, conventional transducer materials, such as magnetostrictive materials, piezoelectric materials, and quantum tunneling composites, cannot be used directly because they are hard, bulky, and noisy.[37] The lightweight, softness, aspect ratio, and minimization of fiber actuators can be easily integrated into a textile structure to fabricate wearable heaters, therapeutic devices, artificial muscles, and drug delivery.[38] According to the operational principles, actuators can be categorized into electric field actuation, thermal actuation, pneumatic actuation, and ion-based actuation.[39] The actuation can further be performed in different forms, such as order, volume, and distance, which diversifies the actuation to various applications, such as bending and torsion.[40]

Thermal actuation: Thermal actuators are actuated by heat, namely, direct heating, electrical heating, electromagnetic or photothermal heating.[41] Thermal actuation is the change in volume or order of the actuator materials. Common materials include semi-crystalline polymers (nylon and polyethylene), phase change materials, hydrogels,

shape memory alloys, and nanoparticle-based films. For polymers, the crystalline regions of the polymer expand and amorphous chain shrinks under thermal treatment. Song et al. fabricated an actuator by incorporating thermoplastic polyurethane (TPU) and CNTs together, where CNTs provided heat via electric current.[42] Another method is to incorporate materials with different thermal expansions to generate bending motion.[43] A coiled polyimide (PI)/PDMS composite yarn actuator demonstrated actuation over a wide temperature range of -50−150 °C.[44] In addition to the materials, different textile structures, such as twist, were applied to the material to maximize actuation.

Electric field actuation: Electric field actuators are based on the electrostatic interaction of electrodes or molecular reorganization within the actuator material.[45] Common materials include dielectric polymers, carbon nanotubes, graphene, ionic polymer metal composites, and conducting polymers. Electric field actuation is dependent on charge accumulation among the materials. Shian et al. designed a gripper made of acrylic elastomers fiber. It can conform to different shapes to move cylinder and grape in the demonstration.[46]

Ion-based actuation: Ion-based actuators are actuated via ion transport within the polymer materials and exchange of ions between the actuator and electrolyte solution. An actuator generally consists of a conductive and ironical membrane sandwiched between the electron-conductive electrodes. Common materials of conductive membranes include conducting polymers and ionic polymers. Wu et al. fabricated an ionic actuator by immersing polyester fabric into poly(vinylidene fluoride-co-hexafluoropropylene) with plasma treatment (PVDF-HEP), and the printed electrode ink was composed of PEDOT:PSS and carbonized carbon nanotubes wired zeolite imidazolate framework-8-composite.[47] It generated a force of 0.62 mN and strain difference of 0.28% at 0.1 Hz.

Pneumatic actuation: Pneumatic actuators are based on fluid pressurization in expandable chambers. They provide linear, torsional, and bending actuation. Cappello et al. designed a textile pneumatic actuator with a sandwiched bladder using polyamide knitted fabric and polyamide woven fabric for producing a glove.[48] The glove generated a force capable of grasping objects weighing 750 g; based on electromyography, user of the gloves did not actively contribute to this. The disadvantages of pneumatic actuators are the requirement of a pump compressor and its non-linear performance.

Additionally, textile actuators face several challenges: Firstly, force and motion generated by the actuator are small. Secondly, Actuation faces a reversibility problem. Thirdly, Actuation is uncontrollable. With respect to textile electronics, many researchers have focused on the development of thermally driven actuators because electric field actuators, pneumatic actuators, and ion-based actuators require additional devices, such as compressors and amplifiers.[45]

2.3 Textile sensors

Sensors detect physical and chemical stimuli to acquire abundant information about the environment as a basis of interaction. Considering the characteristics of textiles, a sensor in textile format can be flexible, durable, biocompatible, and lightweight. The sensors can be used in VR/AR systems as strain, pressure, temperature, gas, smell, and multifunctional sensors. Strain sensors can transduce mechanical motion into an electrical signal to monitor large-scale and small-scale motions; these may find

applications in healthcare, sports, and robotic industries.[49] High stretchability, high sensitivity, quick response time, and fast recovery time are the main considerations of a strain sensor. A strain sensor is mainly fabricated by applying conductive material on a textile structure that was incorporated on a fabric structure at an earlier stage. Huang et al. used PANI, graphene nanoplatelets, and silicon rubber on lycra fabric to fabricate a strain sensor that could sustain 40% strain, and the gauge factor (GF) was 67.3 (**Figure 3a).**[50] As previous sensor stretchability could not reach the 55% suggested by ergonomics,[51] fiber-based strain sensors are being further developed. Lee et al. embedded Ag nanoparticles on fibers, which process 659 GF and can sense 200% strain (**Figure 3b**).[52] Presently, the main challenge of a strain sensor is the trade-off between stretchability and sensitivity because the conductive materials need to be structural and more intact under stretch.[53]

Pressure sensors can detect tactile stimuli and convert them to electrical signals for interaction. They have stringent requirements for sensitivity, resolution, and response time of a sensor. Fabric-based pressure sensors were commercialized at an early stage. A sensor produced using polyethylene terephthalate (PET) microfiber and PEDOT film can sense pressure smaller as 30 Pa and sustain 100 min washing, with a response time of 52 ms.[54] Another capacitive-based pressure sensor yielded a sensitivity of 121×10^{-4} kPa^{-1} with a response time of 7 ms (**Figure 3c**).[55] It was used to detect the pressure of the grasping force. Furthermore, pressure sensor modification focuses on the establishment of a microstructure on the dielectric layer/plate to increase the surface area for sensitivity (**Figure 3d**).[56] However, fiber-based pressure sensors have recently been augmenting. Qi et al. developed a pressure sensor by weaving composite nanofiber yarns (**Figure 3e**).[57] In these composite yarns, Ni-coated cotton yarns were used as the core layer and carbon nanotube-embedded Pu nanofibers were used as the sheath layer. The sensor exhibited a high sensitivity of 16.3 N^{-1} and short response time of 0.03 s (resistive-fiber). Recent research demonstrates that pressure sensor sensitivity is typically less than 10 kPa, which is not sufficient for wearable applications. In future, pressure sensors may be designed with additional functions (e.g., self-powered,[58] self-healing[59] and biodegradable[60]) for advanced applications.

Temperature sensors are essential because core temperature of a human body is among the four vital signals (heart rate, blood pressure, and respiratory rate being the others) for healthcare monitoring.[61] High sensitivity, high accuracy (0.01 ℃), fast response time, good repeatability, and wide operating temperature range (25−40 °C) are the factors that should be considered for wearable temperature sensors.[62] The simple fabrication is to integrate a metallic wire into fabrics or textiles (**Figure 3f**).[63] Another temperature sensor development is using fiber optic sensors. It can provide the required sensitivity and accuracy, but the detecting units are clumsy for wearable applications. In addition, different coatings were applied to textiles to be used as sensors. Cui et al. reported a stretchable temperature sensor by spin-coating a layer of PI resin on the surface of an AgNW film.[64] After curing, laser cutting was used to pattern the cured AgNW/PI layer into the designed Kirigami pattern. The Kirigami structure allowed temperature sensors to achieve constant resistance even at 100% tensile strain **(Figure 3g**).[64] Wang et al. developed a flexible temperature sensor formed by a non-woven calcium alginate fabric with graphene nanoplatelets/sodium alginate coating, which has an accuracy of 0.1 ℃ and sensitivity of -1.5 $℃^{-1}$.[65] To reduce the sensor size and facilitate integration, studies are focusing on fiber-based temperature sensors. A reduced graphene oxide fiber-based temperature sensor has been developed that can sense the temperature in the range of 30−80 °C. It has a short response time of 7 s and

recovery time of 20 s (**Figure 3h**).[66] However, the accuracy of textile temperature sensors cannot be compared with that of commercial sensors, and the performance significantly deteriorates with continuous usage owing to factors such as sweat.

Gas sensors can be classified as optical sensors that respond to gas materials and electrochemical sensors that detect the oxidation of a target analyte.[67] Owyeung et al. developed an optical gas sensor by soaking a cotton thread in a dye solution **(Figure 3i)**.[68] The color information of the thread can be used to detect the existence of an analyte because dyes interact with gas and influence the color. HCl and ammonia gas of 50−1000 ppm were sensed by this sensor. The color of the thread changed at different concentrations of gases. Yun et al. reported an electrochemical sensor to detect NO_2 gas by coating molybdenum disulfide and reduced graphene oxides on cotton fabric (**Figure 3j**).[69] The resistance of the gas sensor changed with the presence of an analyte. Currently, the development of gas sensors faces several problems—first, there is no credible calibration method or system for a gas sensor owing to the transient nature of an analyte. Second, most gas sensors respond to a certain gas, which is a challenge for their application because there are several gases in the environment.[70]

Multifunctional sensation is considered a future trend because it facilitates the miniaturization and comfort of textile electronics. Many researchers have been developing a multi-sensation sensor. Yao et al. presented multifunctional electronic textiles consisting of four electrophysiological electrodes, a strain sensor, and a wireless heater.[71] The fabrication process included coating the AgNW solution on a glass substrate, spin-coating thermoplastic polyurethane (TPU) on top of the AgNW networks, and forming the desired patterns on AgNW/TPU via laser scribing. The resulting textile-integrated AgNW/TPU patterns demonstrated high conductivity (approximately 5030 S/cm).[71] Kapoor et al. developed a woven fabric made of bi-component fiber, which can sense different forces, biopotential, and wetness.[72] The main issue of multi-sensation is signal interference during the process of conducting a decoupling analysis. Apart from sensation, other additional functions, such as energy harvesting, are further preferred for integration in the sensor. Zohair et al. fabricated arm sleeves with Prussian blue active coatings on polyester carbon nanotube threads, which could sense motions and generate power.[73]

2.4 Textile electrodes

Several materials, such as silver fabric,[74] stainless steel yarns,[75] silver yarns,[76] conductive fabric[77] and conductive polymers, such as PEDOT:PSS,[78] and PANI[79] have been adopted to develop textile electrodes. Silver can be coated on different textile substrates, such as yarn or fabric, to develop textile electrodes. To avoid changes in the electrical properties of electrodes resulting from textile stretching, researchers often select textile substrates such as nylon filaments and cotton fibers,[76] which are less stretchable.[80] Apart from the silver yarn developed in laboratories, several commercial conductive yarns composed of silver filaments are widely used to develop textile electrodes. In a study by Ankhili et al., two commercial conductive yarns were investigated: Shieldtex 117/17-2 ply HCB from Statex, Germany and Madeira HC 40 from Madeira, Germany.[81] The two conductive yarns were silver-plated polyamide threads and were embroidered on cotton fabric to develop electrodes for recording electrocardiogram（ECG) signals **(Figure 4a)**. In the structure of textile electrodes, silver yarns are knitted, woven, or embroidered on a textile substrate to form a sensing area.[81-82] Similarly, a stainless steel yarn was also woven in cotton textiles to develop electrodes **(Figure 4b)** in a study by Munteanu et al.[75] In this study, stainless steel

yarns were embroidered on a shirt as transmission wires to connect the textile electrode and rigid readout electronics. Apart from conductive metallic wires and metal-coated yarns, textile electrodes can be fabricated using conductive polymers such as graphene and PEPOT: PSS.[78a] Shathi et al. loaded fabrics into closed flasks with a solution mixed with graphene oxide (GO) and reducing agent.[78a] The reduced graphene oxide (rGO)-coated fabric samples were prepared by placing closed flasks with the samples in an exhausting dyeing machine. Then, the samples were dipped in the PEPOT: PSS solution. The sheet resistance of the fabric decreased from 180 KΩ coated with PEPOT: PSS to 120 Ω coated with PEPOT: PSS and rGO. The textile samples were cut into different shapes, such as squares and circles. In addition, PEPOT: PSS can be screen-printed on a commercial textile to develop an electrode.[83] The printed electrode consisting of a 1 cm round disk was connected to a 1 cm^2 square contact pad. To strengthen the contact between the textile electrode and skin, an ionic liquid was printed on PEPOT: along the area of the PSS active electrode **(Figure 4c)**. Further, pattering method was used to brush PEDOT:PSS on an unprotected textile area.[84] The resultant electrode can be used to record ECG signals during resting and exercise.

A representative property of electrodes is skin contact impedance, which utilizes the user skin properties and features of the electrodes. Based on the observation of the relationship between the contact area and the dry electrode-skin impedance, previous research found that the contact impedance increases when the area decreases.[85] However, there is a correlation between the textile electrodes and quantity of conductive fibers and materials close to the skin.[80] Takagahara et al. reported that when compared with conventional fiber material (fiber diameter of approximately 10 μm) used in electrodes, nanofiber (fiber diameter of approximately 0.7 μm) improves skin adhesion, thus facilitating measurement stability of a biomedical signal.[86] The contact pressure is another factor affecting the contact impedance.[87] The contact impedance decreases as the force from the pressure of the electrode against the skin increases. The results can be mainly attributed to skin adhesion, consequently resulting in a greater effective contact area.[88] Takeshita developed flocked textile electrodes **(Figure 4d and 4e)** and explored the relationship between motion artifacts and contact pressure during an ECG measurement, and found that motion artifacts occurred as the contact pressure between the electrode and skin ranged from 200 to 500 Pa.[89] ECG signals were measured without motion artifacts under a pressure of 1000−4000 Pa **(Figure 4f)**. Considering comfortability, the preferable contact pressure can be 1000−2000 Pa. **Table 1** shows the different materials, fabrication methods, geometrical characteristics, and properties of textile electrodes. Under equal conditions of electrode areas, skin contact impedance decreases when textile electrodes consist of conductive yarns.

3. Textile Electronic Devices for VR/AR

The purpose of the VR/AR system is to help users implement cognitive activity in an artificial environment. In the real world, a human being physically feels the surrounding environment through his/her senses. When a stimulus occurs, specific sensory organs, such as eyes, skin, and nose, transfer the message from the human body via nerve tracks. The efferent nerve information from the receiver organ is transferred to nerve centers, such as the spinal cord and brain. Based on information integration and processing, these centers transfer efferent nerve messages to effector organs, such as ocular muscles, skeletal muscles, and vocal cord muscles. The organs then perform subsequent motor behaviors that produce movements. Based on the approach of a subject's activities, cognitive studies can be conducted to observe the interaction and immersion

in virtual environments. In its absolute sense, it is possible to schematize a subject to be completely immersed in a virtual world.

Sensory stimuli provide people with a coherent perception of the world. Considered as a second skin, textiles are worn on our bodies. Textile electronic devices are an excellent platform for people to simultaneously experience audio, video, allowing haptic, multimodal sensory inputs, and movement in graphically rendered objects or environments.[90] Perception devices transform various perception models in the virtual world to multi-channel stimuli (e.g., tactile, visual, and hearing signals) for detection.[2] This section focuses on textile-based perception devices that convert the virtual perception model of the virtual world into a multi-channel stimulus signal that humans can detect.

3.1 Haptic actions

Haptic perception plays a critical role in enhancing immersion in VR/AR systems by conveying physical interaction with virtual content.[91] Although several haptic devices have been developed,[92] most of the devices are restricted to laboratories or research centers because they are neither wearable nor portable.[93] Recently, several new wearable haptic devices have been integrated in daily life.[94] These devices can be worn or mounted on different human body parts, such as the finger,[95] arm,[96] and foot.[97] To provide a realistic haptic experience, various actuators of haptic devices should be used to produce feedback to the users. The most commonly used actuators are servos, gear motors, pneumatic pistons, and magnetorheological fluids.[98] These actuators are rigid and thus limit the flexibility of haptic devices. The resulting haptic devices are large, bulky, and mechanically complex.

Developing soft actuators is a promising way to improve the flexibility and comfortability of haptic devices.[99] Rogers et al. presented a flexible haptic interface that integrates arrays of miniature vibratory actuators on the sheets of conformal electronics.[8] The developed haptic interface can be directly mounted on the skin. **Figure 5 (a−i)** shows a device with 32 independently controlled haptic actuators. The actuator has a ring-shaped shell that enables the magnet to move freely in the out-of-plane direction. A semicircular area of the magnet was cut on a thin PI disk that was placed on the top surface of the ring. The cut area served as a location for the bonding magnet. The resulting construct could actuate via the interaction of the magnet and current flow through the bottom coil of the ring. The diameter of this type of actuator was approximately 20 mm, and the miniaturized size increased the acceleration of the magnet during vibration. Recently, our group presented a soft actuator consisting of a helical composite yarn.[100] First, plating was conducted to form a metal layer on the PI fiber. Then, PDMS was coated on the surface and in the gap between the composite PI/Cu fiber. Furthermore, the composited PI/Cu/PDMS was used to fabricate helical composite yarn actuators (HCYAs) (**Figure 5j**) with high-temperature resistance. The actuator can achieve tensile actuation of 20.7% under 1.2 MPa stress in the temperature range -50−160 °C **(Figure 5k)**; electrothermal effect was the main driving power. Figure 5k demonstrates that the PI/Cu/PDMS has the highest tensile actuation when compared with those in other studies.

Park et al. utilized the electroactive properties of polyvinyl chloride (PVC) to develop a soft actuator.[99] PVC powder was mixed with a plasticizer and tetrahydrofuran solvent. The solvent became a flat PVC gel after evaporation and was cut into thin and long strings. The PVC strings were then weaved into a PVC gel-knitted fabric. **Figure 5l** shows the soft haptic actuator structure, which consisted of an upper and a lower

layer, an adhesive layer, and a knitted PVC gel fabric. The upper and lower layers consist of a gold plate and PI film, which served as an electrode (20 mm × 20 mm). The dimensions of the actuator were 36 (width) × 36 (height) × 0.8 (thickness) mm. **Figure 5 (m and n)** demonstrates the working principle of a fabricated haptic actuator. When a voltage was applied to the PVC fabric, the PVC chains and plasticizers moved toward the anode (denoted in red), and a force was generated owing to the electrostatic attraction between the two parallel electrodes. Thus, when a voltage supply was applied, the actuator was driven by the combined electrostatic force and electric-field-induced deformation, as shown in **Figure 5n**. Owing to the elastic restoring force of PVC gels, they can recover their original shape when the external power supply is removed. Shape-memory materials can be used to generate activation feedback when they switch between their deformed and initial states.[101] Chernyshov et al. developed a soft haptic device by producing shape memory alloy wires (SMA) for the ring structure and encapsulating it in a silicone tube.[102] The tube was attached to an elastic substrate, such as 3D printed supports. SMA wires were made of nickel-titanium alloy, which shrinks when heated. The fine diameter of SMA wires (150 μm) and their electrical properties enable the development of soft, flexible, small, and lightweight actuator devices. Haptic sense was produced by the pressure from the contraction and expansion of the SMA wire ring. Different electric currents produced different contractions and expansions, which can be controlled by adopting pulse-width modulation or voltage regulation. In future, SMA wires may be knitted or weaved into fabric for the development of soft and unobtrusive actuators.

3.2 Posture and gait tracking

To perform real-time VR/AR activities, the system requires information related to the location and activities of the user. Therefore, term tracking is an important element in VR/AR applications, which is conducted by calculating the real-time orientation and location of users.[103] Gesture and gait recognition is fundamental for tracking techniques. The viewer position changes can be reflected well in the VR/AR-rendered graphics.[104] There are several gesture and gait recognition techniques for detecting and interpreting user gestures and gait. Early gesture and gait recognition techniques used cameras to capture image sequences that were then treated by a processing algorithm.[105]

Recently, several studies have demonstrated that various parameters, such as usability, precision, transportability, and conformability, can be used for motion analysis by employing portable systems with wearable sensors.[106] In the healthcare industry, wearable sensors are attached or worn on different body parts of a patient, such as hand, finger, waist, and foot, to analyze posture and gait. The sensors can be accelerometers, force sensors, gyroscopes, strain gauges, pressure sensors, inclinometers, and goniometers used to measure the characteristics of human motions.[107] Textile sensors are more comfortable and flexible in measuring human postures and movements when compared with other wearable sensors.[108] Textile-based pressure and strain sensors are most widely applied in gesture and gait analysis.[109] This section discusses the basic features and principles of fabric sensors and systems used for monitoring human motions, such as finger, elbow, knee, and ankle bending, with the representative performance of textile-based pressure and strain sensors for human motion recognition listed in **Table 2** and **Table 3**.

According to the mechanism of recognition, various textile sensors for recognizing gestures and gait can be classified into three types: resistive, capacitive, and

triboelectric. Pang et al. designed a fiber-based resistive sensor that can sense various stimuli, such as pressure, strain, and bending, and distinguish multiple gestures.[110] After coating a conductive composite mixture on a polyurethane-silver nanoparticle (PU-AgNP) fiber, the resultant coated fiber underwent a pressure-assisted printing technique to create a hairy structure on the surface of fiber by utilizing the micro-scale cylinder-shaped patterns around the laboratory-made printing equipment. The twisted hairy structures of the conductive fibers resulted in a maximum GF of approximately 1021. Li et al. developed sensing textiles for monitoring human motions of the elbow, underarm, knee, etc.[111] Stainless steel yarns were wrapped using polytetrafluoroethylene (PTFE) and nylon filaments, and the wrapped core–shell yarns were woven into a sensing fabric for the detection of human movements. Capacitive sensors also play an important role in human posture and gait tracking.[112] Yao et al. developed highly stretchable, sensitive, and multifunctional sensors for the detection of pressure (0−1.2 MPa) and strain (0−50%) in less than approximately 40 ms.[112] The fabricated capacitive strain sensor demonstrated several wearable applications, such as monitoring thumb movement, knee joint, walking, jumping, and running. Wang et al. developed a textile capacitive pressure sensing insole for gait pattern analysis.[113] The insole was a sandwich structure consisting of two pieces of conductive textile, which were separated by a non-conductive rubber. Further, two other non-conductive layers were placed on both sides of the sandwich structure as a cover and shock absorber, respectively. Further, textile capacitive pressure sensors measure the force of the toe, forefoot, midfoot, etc.

The aforementioned resistive and capacitive textile-based sensors for gesture and gait recognition require external power supplies to maintain sensor operations. Although the amplitude signals are important indices for pressure and strain sensors to achieve the appropriate finger and knee bending degrees, advanced signal analysis methods are required to perceive complex gestures. To address this issue, self-powered and piezoelectric-based textile sensors have been developed to monitor human motions and scavenge ubiquitous mechanical energy.[114] Advanced methods for signal analysis, such as machine learning and fuzzy inference systems, have been demonstrated as alternative methods to detect human motion. Lee et al. presented a triboelectric textile that can significantly harvest high energy and sense human motion.[115] Pristine textile was transformed into a superhydrophobic textile using a spray-coating carbon nanotubes/thermoplastic elastomer (CNTs/TPE). One of the resulting CNT-TPE textiles was laminated between a nanostructured ecoflex and an encapsulation layer, and another composite textile was covered with an encapsulation layer. A superhydrophobic textile triboelectric nanogenerator (TENG) was employed to monitor human exercise and extract biomechanical energy from humans **(Figure 6a and 6b)**. The power densities demonstrated different values under different motions, such as elbow bending, hand tapping, and running **(Figure 6c)**. Similarly, the output voltages were diverse for different motions **(Figure 6d)**. A 10 μF capacitor was used to store electrical energy generated by treated textile energy harvesting. The collection of electricity can power an electronic watch and calculator, as shown in **Figure 6e**. Furthermore, complex gesture recognition can be achieved through finger motion signal training with machine learning **(Figure 6f)**. After introducing a superhydrophobic surface to the textile generator, the recognition accuracy increased from 92.1% to 96.9% in the sweat condition when compared with that in the untreated generator **(Figure 6g and 6h)**.

The integration of a sensor array has been adopted to detect human grasp signature for manipulating objects.[116] Efforts may be devoted to achieving self-powered sensors by utilizing triboelectric materials.[109b] Advanced signal analysis methods can be introduced in textile sensors for detecting human motion, following which the recognition accuracy of the system can be improved.[117]

3.3 Microclimate control

Thermal sensation of the skin can offer abundant information on the objects and environment via feeling the temperature[118] and microclimate. This section focuses on the relationship between apparel and the human body. Relative temperature is sensed with a light touch on an object; objects are differentiated with various thermal characteristics without any visual cues. Therefore, artificially reproducing controllable/accurate haptic signals with thermal sensation on the human epidermis is a primary research field for the reconstruction of further realistic VR environments.[119] For example, a microclimate control system is required to allow users to experience the same stimulation in cold or hot virtual environments. Textiles, considered as a second skin covering the human body, are ideal platforms for integrating a microclimate control system for achieving an immersive thermal feeling of VR/AR. An ideal microclimate control system consists of textile-based moisture and temperature sensors and cooling/heating devices. The system can sense the physiology of the wearer and environment to provide an individualized simulated environment.[120] Textile-based temperature sensors were discussed in section 2.3. Textile-based heating and cooling devices that require external power are called active systems. These devices can be used to mimic desirable thermal sensations, which are as follows.

Resistive heating is currently a large product area in the interactive textiles and smart fabrics industry.[118] The common structure of a resistive heating textile includes two electrodes and a heating element, which is composed of conductive materials and textiles **(Figure 7a)**.[121] The textile heating devices are supplied with electric power, and the generation of heat occurs immediately when a current passes through the heating elements. Textile manufacturing technologies, such as electrospinning, embroidery, weaving, and knitting, are applied to seamlessly fabricate conductive materials or yarn into the garment.[118, 122] Qiu et al. produced carbon nanofibers (CNF) membranes via electrospinning and carbonization process at 850 °C for 2 h.[123] The resultant CNF membrane was laminated between two PET fabrics to produce a sandwich-structured heating fabric. Infrared radiation nanoparticles (NPs), such as TiO_2 and SiO_2, were integrated into the CNF during electrospinning to enhance the current of the heater. The CNF and wires can be connected to a copper electrode sheet to obtain conductive heating circuits **(Figure 7b)**.[123] The developed heating fabric could increase the temperature from 22−25 °C to 43 °C in less than 1 min under a 30 V voltage. Li et al. researched knitting conductive fibers into a heating fabric.[124] In their study, a heating fabric was knitted with three layers: a front layer was knitted with dielectric yarn, a back layer was knitted with conductive and nonconductive yarns together to generate heat, and a middle layer was knitted with spandex yarn to maintain dimensional stability **(Figure 7c)**.[124c] A geometric model was proposed by extending a sensor model incorporated with a simplified resistive network to predict and compute the resistance of knitted fabric.[125] In applications, the approximate equivalent electrical resistance can be used to predict the heating performance. In addition, Peng et al. developed several conductive fibers by twisting stacked multilayered CNT ribbons, single-ply spring-like fibers, or single-ply nonspring-like fibers, and wove these conductive fibers with copper wires and cotton threads to fabricate heating

textiles, as shown in **Figure 7d**.[126] A textile sample with a heating area of 13 × 10 cm^2 was subjected to different voltages (5, 7, and 9 V), and the saturated temperatures increased (to 38, 48, and 60 °C, respectively) in approximately 100 s **(Figure 7e)**.[126] Furthermore, embroidery of heating elements is integrated during textile fabrication, providing advantages such as a variety of applications and freedom of design.[127]

Roh et al. designed and fabricated four different circuits for heating by embroidering metal composite embroidery yarn (MCEY) on a textile substrate.[118] The four prototypes have equal resistance but different cover factors. One of the heating textiles and its performance are shown in **Figure 7f**. In this article, cover factor refers to the ratio of heated area to unit area. A higher cover factor has a smaller temperature range. The relationship between the cover factor and average surface temperature was explored. It can be used to guide the structure design in heated embroidered circuits. Nonconductive textiles are used as substrates to coat conductive materials such as gold, AgNWs, PEDOT, PEDOT:PSS, PPy, CNT, and graphene, and the resultant conductive textiles are used as heating elements.[127-128] Wang et al. introduced in situ polymerized PPy on metal carbides/nitrides (MXenes) surfaces to develop robust inks for textile coatings to improve the electromagnetic interference shielding efficiency.[128b] Moreover, a silicon-film layer was coated on the PPy/Mxene-decorated textile for waterproofing. Considering the silicone-coated M-textile (1 × 4 cm^2), the Joule heating performances were compared under different input voltages.[128b] There was no significant temperature variation was detected at a voltage of 1 V. However, the saturated temperature increased at a voltage of 2 V (approximately 40 °C), and the temperature was further increased to 57 °C at 3 V and 79 °C at 4 V.

Textile cooling systems are generally developed by integrating liquid cooling and thermoelectric (TE) cooling.[129] Kotagama presented soft, liquid-cooled tubes composed of aluminum particles, which can control the temperature at 10−50 °C for a cooling jacket.[129a] The developed cooling tubes can be embedded in personal, robotics, or wearable electronics for cooling.[129a] Hong et al. utilized thermal devices (TEDs) to reduce the cooling volume; flexible TEDs can offer a cooling effect of greater than 10 °C.[129b]The TED structure was connected with TE pillars using flexible copper electrodes and sandwiched between stretchable sheets **(Figure 7g)**. **Figure 7h** illustrates a cooling armband integrated with a flexible battery pack. The device was examined under realistic conditions of walking, sitting, and running to investigate the effects of metabolic conditions and different convection, as shown in **Figure 7i**. The maximum temperature of the skin cooling effect was 6 °C.

The integration of heating and cooling temperature control in one device may reduce the thermal device weight and improve comfortability. Recently, Ko et al. developed a bi-functional (cold and hot sensations) thermo-haptic device that actively heated up and cooled down deformable skin surfaces.[119] **Figure 8a** provides a simplified illustration of the internal structure of a thermo-haptic device. One side of the Cu electrode was coated with polyimide (PI), and a thin thermally conductive elastomer film was then used to encapsulate the PI. Another thermally conductive elastomer layer with holes was coated on the other side of the Cu electrode. The resultant multilayer materials were placed on top of the thermoelectric layer, which consisted of p-type and n-type Bi_2Te_3 thermoelectric materials. The remaining multilayer materials were placed at the bottom of the thermoelectric layer. **Figure 8b** shows the final design of the thermal haptic device, which can cool down or heat the body surface via a simple switch in the direction of the electric current. To explore the cooling and heating performance of the thermal haptic device, an increasing current was applied at a 20 s interval. **Figure 8c**

shows the time-dependent temperature curves and corresponding infrared camera temperature images. The results showed that in both working modes (cooling and heating), the thermal haptic device generated a satisfactory temperature with fast response and highly controllable and bi-functional performance.

Effective heating or cooling systems are very helpful in VR environmental conditions. For example, higher temperature gradients would be required to allow firefighters or mountaineers to experience fire or snow in VR environments. Thermoelectric textiles can be potential research subjects for developing switchable heating and cooling. Most of the existing textile-based comfort thermal systems pose challenges when employed in VR environments because of the narrow temperature range and high-power requirement.

3.4 Olfactory and gustatory perception

Human smell (olfactory) and taste (gustatory) senses rely on chemoreceptors that respond to chemical stimuli. Olfactory detects chemical molecules in the environment, while gustatory provides feedback on taste. The olfactory and gustatory systems have less impact on the presence and immersion of VR systems; hence, their development is backward when compared to that of visual, auditory, and haptic detection.[130] Textile-based gas sensors can be integrated into VR/AR systems to provide olfactory feedback and enhance the immersion of different training scenarios. Gas sensor arrays are a promising method to detect volatile gases in our environment.[70] Gustatory simulations are mainly developed for entertainment or research purposes. Narumi et al. presented a pseudo-gustatory display to allow users to experience different food tastes without changing their chemical composition.[131] The results demonstrated that the system can change a perceived flavor, allowing the user to experience different flavors by changing the olfactory and visual messages instead of the chemical composition of flavors.

3.5 Surface bio-potentials of brain and muscle activities

Surface biopotential signals from the human body can be measured using electrocardiogram (ECG), electrooculogram (EOG), electroencephalogram (EEG), and electromyogram (EMG). They have been investigated as inputs for VR/AR systems. For example, EMG has been used to control and drive an artificial arm for the rehabilitation of stroke patients.[132] EEG is commonly used to check the impact of visual stimuli on the level of brain wave activity,[133] decode the attention state of the user during an AR paradigm,[134] and evaluate psychophysical effects associated with VR/AR systems.

Popular EEG systems in the VR/AR system integrate multichannel cables and electrodes on a head cap. Electrodes are essential elements of an EEG cap that couples biopotential signals from the human body to the front-end amplifier. Present biopotential electrodes can be grouped into three classes: wet, dry, and non-contact. A conventional wet electrode consists of silver−silver chloride (Ag/AgCl) metals surrounded by wet and/or solid hydrogels with chloride. In a dry electrode, the metal is in physical contact with the skin to couple biopotential signals without using explicit gel/wet coupling media. Another contactless electrode collects signals through an insulation layer, such as a nonconductive textile layer or air without direct skin contact.[135] This is an ideal working condition for smart textiles to detect surface biopotential signals in daily life, neonatal units, or be integrated into beds and chairs.[80] Textile electrodes have several advantages: they lack hydrogel, are biofriendly, and are comfortable for long-term monitoring. However, there are several challenges in

combing textile electrodes for measuring biopotential signals in the VR/AR system. First, when a user puts on an EEG cap, he/she must wear a VR headset over the cap as the VR headset applies pressure to the sensors, displaces the sensors and twists the cables, which leads to poor data quality. Second, the comfortability of textile electrodes can be counterbalanced by the decreased robustness to motion and noise artifacts. The two aspects are major limitations that hinder the broad applications of the VR/AR system with innovative electrode technologies.

EMG is an electrodiagnostic technique used to evaluate and record the electrical activities of skeletal muscles.[136] Based on the EMG sensor type, EMG devices can be classified into two types: needle EMG and surface EMG. Needle EMG adopts needle electrodes that are inserted into the muscle of interest to measure action potential. Surface EMG uses invasive electrodes that attach to the skin surface to monitor neuromuscular disorders. The applications of EMG include rehabilitation, ergonomics, prosthetic devices, and sports science.[137] EMG can utilize textile platforms because the platforms collect real-time data via a realistic and casual approach. Studies on EMG-recording adopted textile electrodes focus on two aspects: demonstrating the feasibility of developing new electrodes for the desired applications, and researching integrating textile electrodes in wearable garments.[138] Pino et al. developed a smart shirt integrated with textile dry electrodes to record EMG in the upper limbs.[139] Other wearable EMG systems fitted with textile electrodes have also been demonstrated, such as running leggings for detecting muscle fatigue,[140] shorts for analyzing energy expenditure,[141] eyeglasses for chewing cycle detection,[142] and a shirt for physical exercise training.[139]

Research has been increasingly focusing on the interaction between brain activities and VR/AR system. The interaction can be classified into two types: passive and active. Passive interaction indicates that the VR/AR systems sense stimuli or signals from the brain and respond appropriately. EEG is a common brain activity detection method that detects a user's emotion and consciousness in the system and the reaction for an appropriate response.[133] Through the brain sensation, the interaction and performance of the VR/AR system become further diversified and abundant.[143] Sensation is considered the first step in the development of customized and smart VR/AR systems. Active interaction indicates that the control of VR/AR systems is directly realized by the brain, eliminating the requirement of other electronic devices, such as the mouse and keyboard.[9] The active interaction aims to normalize the control or interaction of a VR/AR system to be more harmonized and humanized, thus delaminating the distraction caused by inconvenience during its use. The brain VR/AR system can relieve the hands and other body parts of a user for a simpler and more direct interaction, such that the user is more attentive to the interaction.

Combining brain–computer interfaces (BCIs) with VR/AR technologies has been achieved by developing a system that provides immersive images to users and feedback generated by using the BCIs in real-time.[144] Wearable textile electronics significantly facilitated the application of bipotential monitoring in the fields of human−computer/machine interaction (HCI/HMI) and BCIs. Textile-based BCIs is a new input device to the VR/AR system as the BCIs may completely change the system interactions with virtual environments. In addition, textile-based BCIs are more intuitive when compared with conventional devices.

4. Fabrication of Textile Electronic Devices and VR/AR Systems

VR/AR are multidisciplinary technologies and integrated systems, including devices such as personal computers, and consoles/smartphones, which are used for sequentially processing inputs and outputs. Further examples include input devices that provide users a sense of immersion, output devices that can provide audio, visual, smell, tactile, and other stimuli for the generation of immersive feelings, and software that has a responsibility for input/output device management, incoming data analysis, and appropriate feedback generation. VR technology completely immerses a user in a synthetic environment without having to look at the real environment. AR technology enhances the feeling of reality by superimposing virtual objects with real-time interaction with the real world. Because the VR/AR systems combine the physical real world and a virtual world, data transmission among different components and the corresponding responses must be accurate and timely to maintain the feeling of immersion. This section explains the coupling of VR/AR with the devices and related electronic interfaces to develop a more intuitive and wearable VR/AR system that can provide a natural user experience.

4.1 Fabrication of textile electronic devices

To fabricate different textile electronics with advanced electrical and textile properties, researchers have explored different fabrication methods. The techniques can be generally categorized into two groups: physical methods and chemical methods.

4.1.1 Physical methods

Physical methods tend to control the deposition or etching of materials for textile electronics without chemical reactions. The general physical fabrication methods can be summarized as spinning, printing, coating, physical vapor deposition, and carbonization. The printing method has the advantages of low temperature, non-vacuum operation, low production cost, potential for large-scale manufacturing, and wide compatibilitywith materials.

Spinning. It is an efficient approach to produce intrinsic conductive fibers by ejecting a polymer solution throughout the spinneret, followed by solidification. It is commonly categorized into wet spinning, melt spinning, and electrospinning. Wet spinning was investigated to produce conductive fibers from polymers, such as PANI, PPy, and PEDOT:PSS, by dissolving the polymer in a solvent. The improvement of the conductive fiber properties is realized by mixing a non-conductive polymer in the solution. Gao et al. developed a composite fiber from PEDOT:PSS and polyvinyl alcohol (PVA) via wet spinning.[145] The composite fiber demonstrated better mechanical properties than pure PEDOT:PSS. Its electrical performance remained stable after 140 cycles at 20% strain. Wet spinning and melt spinning can produce conductive fibers by mixing conductive materials directly in the polymer solution. Kim et al. used the wet spinning method to produce polyurethane (PU)-silver/graphene composite fibers, whose conductivity was as high as 82874 S/m with 150% strain.[146] Potschke et al. fabricated a fiber from poly(lactic acid) with a multi-walled carbon nanotube to detect different solvents/liquids, such as methanol, ethanol, and n-hexane.[147]

Electrospinning has the advantage of producing nanometer-scale fibers, where the fiber formation is controlled by an electric field. Huang et al. electrospun PEDOT:PSS using magnesium nitrate as the physical cross-linker in nanofibers; the PEDOT:PSS produced was used to fabricate gas sensors to detect organic gas.[148] Mixing conductive and nonconductive polymers is being studied in several developmental studies. Low et al.

mixed PANI and poly(caprolactone) (PCL) polymer solution with different aspect ratios to form a nanofibrous gas sensor for NH_3 and NO_2.[149] Fabrication of non-conductive fibers for further treatment is another pathway for development. Yang et al. fabricated a conductive electrode based on an electrospun poly(4-vinylpyridein) polymer network with the deposition of Cu.[150] The sheet resistance was 15.6 Ω/sq.

Screen printing: This method is operated by using a squeegee to press the ink passing through the stencil to form a pattern on the conductive substrate. Common inks used in this method include metallic ink (Cu, Ag, and Au), carbon ink, and conductive polymer solution. Researchers have applied screen printing for textile electronics owing to large-scale manufacturing and reproducibility of the high aspect ratio of patterns.[151] For instance, Ke et al. screen-printed Ag nanowires as electrodes on a fabric with a sheet resistance of 1.5 Ω/sq.[152] The electrodes can sustain 200 cycles strain with no significant loss of conductivity. Screen printing is further utilized to pre-treat the substrates for other fabrication methods. Mao et al. used screen printing to print dopamine on the polyester fabric, which was followed by the reduction of silver and electroless plating.[153] Higher viscosity ink in screen-printing leads to a more integrated and firmer conductive track. However, it also deteriorates the breathability and flexibility of the textile substrate. The low resolution of the pattern limits its application.

Inkjet printing: Inkjet printing ejects a fixed quantity of ink from the chamber, passes through the nozzle onto the substrate. The common inks used in this method include metal ink (Ag, Cu, or Au), rGO ink, ICPs, and CNT.[154] The main challenge in the method is that the porous structure may break the continuous conductive track. Stempien et al. printed eight layers of silver ink on textile fabrics to realize a 0.155−0.235 Ω/sq conductivity.[155] The application of inkjet printing in antennas, heating actuators, capacitors, and transmission lines was prototyped. Continuous improvement to the ink, printing parameters, and process developed the application of inkjet printing to a more porous fabric. Shahariar et al. printed reactive particle-free silver on polyester knitted fabrics using in-situ heat curing.[156] The fabric minimum sheet resistance was 0.9 Ω. Apart from changing the nozzle size to improve the resolution, different techniques were incorporated in inkjet printing, such as the electrodynamic jet technique and selective laser sintering process.[157] The limitation of inkjet printing is nozzle clogging, the formation of a coffee ring, and low electrical conductivity of the track due to the low viscosity of the ink.

Aerosol jet printing (AJP): AJP is an additive printing method based on aerodynamic focus used to produce high-resolution deposition of colloidal suspensions. During printing, liquid ink is first atomized into mist by a pneumatic or ultrasonic system. The atomized material is then transported to the nozzle via gas flow and focused inside the nozzle via a sheath gas. Then, the atomized ink is jetted out the nozzle onto the substrates placed at a distance of 3−5 mm from the nozzle. The advantages of AJP include diverse applicability of substrates and ink and no nozzle clogging. The printed materials include metals, conductors, insulators, oxides, polymers, and biological materials. A substrate includes both the planar and nonplanar substrates, and two-dimensional (2D) and 3D objects. Agarwala et al. fabricated a strain sensor using AJP to print silver ink on the bandage to monitor human joint movement, which can withstand 700 cycles at a radius of 5 mm.[158] The limitation of AJP is that it has a printed pattern of sprinkles and waves owing to its mechanism, and sharp edges cannot be obtained. AJP has been applied to flexible displays, transistors, circuits, and sensors.

However, presently, most devices are film-based or paper-based. The application of AJP to textiles requires further development.

Coating: Coating applies a semi-liquid material to one or both sides of a textile. For textile electronics, coating can directly convert already manufactured non-conductive textile products (fiber, yarn, and fabric) to conductive textiles without the integration of electronic materials or functionalities during the manufacturing process. It provides more freedom to the design of electronics and applicability of materials. Therefore, different coating methods and coating materials must be developed. The primary importance of coating is the adhesion between the substrate and coated materials, which is significantly influenced by the wetting of the substrate and adhesion of the material to the substrate. Common coating techniques used for textile electronics are dip coating, in situ polymerization, and spray coating.

Dip coating: Dip coating is achieved by immersing a substrate in a conductive solution, withdrawing it at a controlled speed, and drying it. The main consideration of dip coating is that the conductive materials are evenly distributed inside the solution, and aggregation does not occur inside the solution. For textile electronics, many conductive materials were dip coated on the substrate to realize different functionalities. He et al. fabricated a new nanogenerator using a simple dip-coating method to coat PEDOT:PSS on cotton fabric, which was used to detect body motion and harvest energy.[159] The main limitation of dip coating is the variation in smoothness and uniformity.[160] Hence, dip coating is modified to enhance the coating on a textile substrate with different equipment, such as vacuum- and spin-assisted dip-coating.

Spray coating: Spray coating is appropriate for low-weight substances. During the process, the coated materials are placed in a pressurized vessel and on a substrate with a high-pressure air stream that flows from a nozzle.[161] Khattab et al. spray-coated dysprosium and europium-doped strontium aluminate phosphor on a woolen fabric to endow photoluminescent properties on the fabric.[162] Gong et al. spray-coated PEDTO:PSS on PET fabric, whose minimum sheet resistance was 12.1 Ω.[163] Uniformity of coating is the major limitation of spray coating.

Physical vapor deposition (PVD): PVD is a vaporization coating process, where coating materials transform into different phases (gas, liquid, and solid) throughout the process to form deposition on the textile surface. The coating thickness is generally less than 10 μm.[164] PVD can be categorized as sputtering, vacuum deposition (evaporation), arc vapor deposition, and ion plating; sputtering and vacuum deposition are more commonly used techniques. Sputtering can deposit wide coatings on textile substrates, such as polymers, metals, and metal oxides, with good adhesion. In addition, it can be employed to deposit coatings with several layers.[165] In the production process, it is suggested to knock off atoms from a solid material because of the target bombardment by energetic ions.[166] The ejected molecules or atoms have a certain orientation and kinetic energy that causes them to condense onto the substrate for the formulation of a thin film. Wei et al. coated copper on polymer fibers via sputtering; the resultant electrical resistance was very high (250 Ω/cm).[167] Jiang et al. coated copper on polyamide-6(PA-6) fibers via sputtering and achieved an electrical resistance of 7.03×10^{-5} Ω/m.[168]

4.1.2 Chemical methods

Chemical techniques involve chemical reactions to modify the textile surfaces of conductive materials by adding chemicals or controlling the chemical components of a

substrate.[169] The common chemical fabrication methods include plating, chemical vapor deposition, and carbonization.

Plating: Plating is based on electrochemistry, which can be used on different textile structures, such as fibers, yarns, and fabrics. It can be categorized into electroless plating and electroplating.

Electroless plating: Electroless plating occurs in an aqueous solution based on a chemical reaction without any electrical power supply.[170] It is preferred for the fabrication of textile electronics because it can directly transform non-conductive textile substrates to conductive substrates. In an electroless plating bath, the presence of a reducing agent releases hydrogen to produce a negative charge on the surface of textiles.[171] Then, the metallic ion inside the solution reduces from the metal layer on the textile substrates. The thickness of the electroless plating is 1−130 μm.[170] As electroless plating can directly convert non-conductive textiles into conductive textiles, it is used to develop textile electronics devices. Ma et al. fabricated a strain sensor by plating a silver layer on a cotton/spandex blended fabric with a gauge factor of 26.11 and robust electrical conductivity of 15.7 S/m.[172] During the development of electroless plating, different pre-treatment methods, such as plasma treatment and chemical etching, were applied to the textile substrate for adhesion. Park et al. developed a Cu circuit on PET substrates with plasma treatment, which improved the adhesion of the plated material to the substrate.[173] The adhesion was tested to be as high as 38.53 N/m. As the plating is not a selective addition fabrication method, other pre-treatments, such as tie-dying,[174] wax dotting,[175] and photolithography, should be incorporated for patterning. Zhao et al. used wax-dot printing to form a Cu pattern on cuprammonium fabric, where the minimum width of the track was 400 μm with a resistance of 7.52 μΩ cm.[175] The main advantage of electroless plating is that the plated layers are uniform throughout the textile, but an increase in the thickness of the coating increases the hardness and brittleness. Further, its chemical solution is hazardous, toxic, and not environment-friendly.

Electroplating uses electric current to drive the reduction of metallic ions on textile substrates. For electroplating, the substrates act as cathodes in an electrolytic bath. A low voltage current is passed through the solution that deposits metal on the substrates.[176] The coating of electroplating is in the range of 1−1000 μm.[170] Electroplating requires that the substrate is conductive; however, most textiles are non-conductive. Thus, electroplating is not an appropriate fabrication method for textile electronics; it is mainly used for the performance improvement of produced textile electronics by increasing the thickness of the conductive layer. Ali et al. electroplated silver on a copper-coated fabric to improve its conductivity from 70 Ω mm to 2 Ω mm, which can be used to fabricate a triboelectric generator to generate a current of 33 V and 6 μA under pressing.[177]

Chemical vapor deposition (CVD): CVD relies on chemical reduction to deposit gaseous chemical precursors on textile surfaces.[178] It can be initiated by different forms of energy, such as heat, plasma, or light. In CVD equipment, initiators and different monomers/precursors are transported into its chamber in gaseous forms.[179] Then, the monomer and initiator bond to the substrate and conduct a reaction to form a conductive layer. The by-product is then exhausted. In the early stages of the CVD development, the process was generally initiated at least 200 °C; the scope of its application was limited to certain polymers.[180] Further, plasma-enhanced CVD was developed, which significantly lowered the initiating temperature. While short

wavelengths can damage chemical bonds, their application to textiles is limited. Bashir et al. fabricated a conductive viscose yarn via oxidative chemical evaporation to deposit PEDOT on its surface.[179] In addition, there is limited research on using CVD on textile substrates.

In-situ polymerization: It is described as the polymerization in either the gas or liquid phase in the presence of the desired substrate. A textile substrate can be immersed in the solution or gas containing monomers, and the addition of oxidant initiates the monomers to form a long chain as a polymer. The general polymerized materials include pyrrole, PEDOT, and other ICPs. The advantages of in situ polymerization are: the mechanical properties are barely affected and potential for large-scale production. Lv et al. converted normal textile fabric into sensing textiles by polymerizing a thin PPy layer on the fabric surface at a low temperature.[181] The electrode demonstrated the highest specific capacitance of 4848 $mFcm^{-1}$ at 1 $mAcm^{-2}$. Real-time control and reproducibility of in-situ polymerization hinder its development.[160] The polymerization solution can damage the textile because of the presence of acid, pyrrole, and aniline.

Carbonization: Carbonization is a thermal treatment used to anneal the textile substrate in an inert atmosphere to produce carbon fiber/textile. The common precursors are PANI fiber and pitch. During production, the precursor is first oxidized in air at 200−300 °C. Then, carbonization is applied in inert surroundings at 350−1700 °C to remove a majority of non-carbon atoms, such as nitrogen, oxygen, and hydrogen. The temperature is continuously increased to more than 2000 °C, as graphitization, to form a graphite structure and heal its structural defects.[182] The carbon fibers have a proportion of more than 90 wt.% carbon, with a higher tensile strength of 2−7 GPa and tensile modulus (200−900 GPa).[183] Further, different microstructures and microscopical carbonized fibers were developed to increase the surface area for energy storage and electrocatalysis. Zhu et al. encapsulated liquid metal inside hollow carbon fibers, which were employed in lithium-ion batteries as an anode with a reversible capacity of 552 $mAhg^{-1}$.[184] Apart from PANI and pitch, lignin and other materials have been utilized for carbonization. Li et al. developed a supercapacitor based on a hollow carbon textile, resulting in high capacitance (maximum 220 Fg^{-1}).[185] The tensile stress of the carbon textile was 1.3 MPa and its elastic modulus was approximately 26.5 MPa. The properties deviated from the PANI-based carbon fiber. As carbonization completely influenced the chemical and physical structures of the materials, the textile properties of the original materials deteriorated. The dimensions of the fibers after carbonization decreased, following which the surface area decreased to 49.2% and weight decreased to 84.7%.[186] Further, carbonization causes pollution: it produces toxic gases such as NH_3 and HCN at temperatures lower than 700 °C.[30]

4.2 Electric interface of textile VR/AR system

The electric interface of a textile VR/AR system consists of signal conditioning, microcontroller, and wireless module for data processing and display.

Signal conditioning is the manipulation of an analog signal to satisfy the requirements of further processing. Limited by the maturity of the manufacturing technology, the output signals of textile devices cannot be directly sent to analog/digital converters (ADC). Thus, signal conditioning is required to convert the obtained data from the textile device to practical output. A resistance-to-voltage conversion for resistive devices is generally used to convert resistance variations to a voltage signal owing to its simple structure.[187] Bridge circuits are not suitable for textile resistive sensors

because of their large resistance range and calibration requirement for zero output before their usage. To address this problem, Shu presented a signal conditioning circuit consisting of a group of voltage dividers and a single-element bridge circuit **(Figure 9a)** for a textile resistive sensor.[188] The system functions of a voltage divider and single element bridge were also explored. After signal conditioning, voltage signals were delivered to analog/digital (AD) channels. The multi-channel sampled values were processed in a microcontroller. In addition, an adequate interface is required to convert data collected from textile capacitive devices to available signals for processing. Ma et al. presented an interface method for transmitting signals of humidity sensors to mobile terminals.[189] **Figure 9b** demonstrates the interface circuits consisting of a transformer, rectifier filleter circuit, stable voltage circuit, sensor, PCAP01-AD, microcontroller unit (MCU), and mobile device. The transformer, rectifier filter circuit, and stable voltage circuit served as power supplies to the AD. The output signal from the sensor was transferred to PCAP01-AD, which was a capacitance-to-digital converter. The digital signal was then sent to the MCU for signal processing. The interface adopted wireless transmission to transfer data from the MCU to the mobile device.

Although the development of textile electronics is growing rapidly, research on signal conditioning circuits of textile-based devices faces challenges. Presently, a standard circuit does not exist for converting textile device signals to voltage signals that can be recognized by AD. Generally, researchers design and develop signal-conditioning circuits, and these circuits often have low integration levels. The resultant circuits are bulky, rigid, and fragile, and cannot be used in practical applications of textile electronics. The controllers, ADC, and wireless modules are rigid commercial components. Although their sizes are being miniaturized, their functions are becoming increasingly complex. Suitable electronic components can be selected by comparing their performances, such as function and energy consumption.

4.3 Energy supply and management

Electricity is essential to drive components such as textile devices and electric interfaces. Harvesting the consumed energy from our surrounding environment could be an ideal approach to address the power supply issue of wearable VR/AR systems.

VR/AR devices vary from simple mechanical additions of existing electronics to full-fledged dedicated devices, which promise an enhanced experience to users. The main components of VR and AR systems, such as display units, controllers, AD converters, wireless modules, sensing units, and computing units, can work separately or simultaneously. Therefore, different power supplies and management strategies should be employed in the design. Displays, computers, and related electronics made of solid hard materials are rarely fabricated in textile structures, but soft textiles can be utilized in their external packages for comfortability. Moreover, their energy supply can be enhanced by wearable generators that harvest energy from human motions and fabricated in textiles using the textile processing approach (wearing, sewing, knitting, laminating, etc.).

Textiles can be versatile design carriers for flexible and wearable electronics because they are considered a necessity and have a large size. Extensive demonstrations of integration between advanced generator technologies and textiles have been reported to harvest energy from human motions.[190] The maximum available energy exists on the lower limb motion, such as the knee (33.5 W), ankle (18.9 W), and hip-joint motion (7.22 W), and heel strikes (1−10 W).[191]

Wearable generators harvest ambient energy based on the thermoelectric, photovoltaic, electromagnetic, piezoelectric, triboelectric mechanisms, and their hybridization have been regarded as an alternative approach for the replacement of batteries.[190e, 190f, 192] The most common transduction mechanisms for transforming thermal and solar energy to electric power are thermoelectric and photovoltaic effects. Zeng el at. assembled a reduced graphene oxide film on 3D printed polydimethylsiloxane grids for fabricating a flexible thermoelectric generator. It was demonstrated in a wristband-type flexible thermoelectric generator with a high-power density of 4.19 μW/g. The surrounding temperature difference is less than 15 °C.[192c] Zhang et al.. further proposed a theoretical method for predicting the performance of 3D fiber-based thermoelectric generators, which consists of a single-dimensional fiber generator array that functions under the condition of radiative and conductive heat transferring at a low level of temperature variation.[192d] Such methods are advantageous as they do not require relative movement or deformation, exhibit disadvantages of low efficiency, and are easily limited by their surroundings.[6]

In contrast, harvesting mechanical energy based on piezoelectricity, triboelectricity, electromagnetic, and/or electrostatic induction has fewer limitations from the surrounding environment. Meanwhile, the harvesting structures have become complex in textiles. Textile-based piezoelectric generators can be fabricated in extremely compact structures, such as those of functional fibers, which have been extensively developed. Fiber-shaped energy harvesting devices contribute unique benefits to portable and wearable electronic systems.[193] However, the performance of the fiber-based generator is low. Soft textiles cannot provide sufficient compression on the piezoelectric units. The TENG can work with a very low level of applied force, higher surface charge density, and high output power.[190d, 190k] Dong et al.[194] recently summarized the outputs of textile-based piezoelectric and triboelectric generators, indicating that the output voltage, peak instantaneous power, and peak instantaneous power density of textile-based piezoelectric generators are in the range of 1 mV−48 V, 10 nW−1.42 mW, and 0.15 μW/cm^2−125 μW/cm^2, respectively. The output voltage, peak instantaneous power, and peak instantaneous power density of the fabric-based TENGs are in the range of 3 V−~ 2,000 V, 0.016 mW−21 mW, and 8 μW/cm^2−176.8 μW/cm^2, respectively. The highest peak instantaneous output power density (176.8 μW/cm^2 at a balanced load of 50 MΩ) is achieved by a textile energy harvester depending on the single-electrode mode TENG at a relatively high force of 1200 N and an effective area of 56.7 cm^2. [195] Such a generator generally charges a 200 μF commercial capacitor storage device that is employed with a bridge rectifier. When compared with the practical applications, the harvester shows a low charging capacity with 6.7 mV/s at 100 N and 11.3 mV/s at 1400 N. Tao el at. summarized the performances of representative textile-based energy harvesters by comparing different types of generators, including electromagnetic, piezoelectric, triboelectric, thermoelectric, photovoltaic, and hybrid generators, and showed that electromagnetic generators demonstrate the highest output power of approximately 32 mW.[6] To date, electromagnetic generators have rarely been utilized in wearable textile-based harvesters because of the high moving speed of relative movement of coils and magnets; the generators also heavy.

Hybrid generators showed a higher output power of approximately 222 μW/cm^2 from the triboelectric and piezoelectric units[190d] and 320 μW/cm^2 from the triboelectric and solar cell units.[193b] Their output power is higher than those formed by a single mechanism. However, the harvested energies may not be sufficient to power

commercial VR/AR systems. For example, the capacity of batteries utilized in commercial VR/AR products is several thousand mAh, such as 550 mAh−800 mAh of the head-mounted display devices used for industrial augmented reality systems.[196] The average power is several thousand mW.[197] Thus, further improvement of the output power of the generators and maintenance of the mechanical benefits in textile structures should be conducted for future development in energy harvesting.

VR/AR systems include several components. Each component can work separately and with other components through wireless/wired communication technologies. The power consumption of a VR/AR system is high, but that of a single component can be as low as a few hundred mW of power, or several μW, such as the average power consumption of an electric watch (approximately 1 μW) and smoke detector (approximately 6 μW).[198] Most VR/AR systems are powered through batteries and wireless methods for the systems to be portable. A series of self-powered sensors or controller components for VR/AR systems have been developed. A triboelectric nanogenerator has become a promising system for application in self-powered sensing and energy harvesting.[199] A fabric-based triboelectric generator can be used as an internal power source to demonstrate the self-power operation of light-emitting diodes, liquid crystal display, and keyless vehicle entry system.[200] An all-textile triboelectric sensor-based smart glove was developed that was capable of capturing human gestures for remotely controlling a VR that enabled a teleoperated robotic gripper.[201] Such a self-powered sensor can perceive human motions in a broad pressure-sensitive range (100−400 kPa) and high sensitivity of 1.1 V/kPa. Similarly, a glove-based self-powered intuitive interface has been developed based on triboelectric nanogenerators, which consists of a PEDOT:PSS-coated textile strip sewed on a glove and silicone rubber thin film layer coated on the glove.[114b] The aforementioned self-powered systems are required to store electricity in a capacitor or battery first, and then power the wireless modules; this system lacks continuous and long-lasting workability. Battery-free components can be employed to reduce the energy consumption of VR/AR systems. For example, the application of TENG-based direct sensory transmission was demonstrated on a battery-free short-range self-powered wireless sensor network that was further utilized in a 2D multiple-freedom-degree toy car control and 3D VR drone control with a single coil.[202] Apart from TENGs, other technologies can be utilized for self-powered systems: a wireless and battery-free platform has been developed for haptic interfaces and electronic systems, which can be softly laminated on the curved surface of the skin for information communication via spatiotemporally programmable patterns of localized mechanical vibrations.[8] Such self-powered devices can add sensations of touch in the AR and VR. The technology has certain drawbacks of demonstrating a large current (~5 mA) and high-power consumption (~1.75 mW of an optimized actuator), which is a critical limitation to sustainably and wirelessly operate a VR/AR platform.[8, 203]

Supercapacitors (SCs) and batteries have become flexible and can be fabricated in fiber-shape. SCs exhibit excellent power density, long cyclic stability, and immediate charge-discharge rate. When compared to SCs, batteries store energy by converting electrical power to a chemical form and demonstrate low self-discharge properties, high working voltage, and intensive energy density. The existing separators, electrodes, collectors, and electrolytes have a similar composition to textile-based SCs and batteries. According to the device configuration, the SCs and Li-ion batteries are fabricated in 1D fiber/yarn structures and 2D fabric architectures. Zheng el at. reported a new technology for additive functionalization and embroidery manufacturing that allows textile-based

SCs to be fabricated in knitted, woven, and nonwoven fabrics with power densities ranging from 1.1 mW/cm^2 to 2.0 mW/cm^2.[204] A fiber-shaped PEDOT@MnO_2//C@Fe_3O_4, which is an asymmetric SC used for fabricating wearable electronics, was developed by Sun et al.. It demonstrated a working voltage of 2 V, real specific capacitance of 60 mF/cm^2, and an energy density of 0.0335 mWh/cm^2.[205] The integration is used for fabrication in all-in-one SCs as an anode, a cathode, separator, and current collector, which are integrated in one monolithic glass fiber substrate and other circuit components by adopting scalable and mature fabrication techniques. The all-in-one SC that delivered a high energy density (2.12 mWh/cm^3 and power density (320 mW/cm^3) is embedded as a component for 3D electronics, and performs a 100% capacitance retention even after a 431 h continuous cycling operation.[206] Tao et al.[6] and Kim[207] recently summarized the progress of textile-based energy storage devices and showed that although momentous accomplishment was achieved in recent years, the electrochemical performance of the device, including power and energy densities, capacity, durability, flexibility, cycle stability, scalability, safety, and device integration issues, requires improvement for VR/AR applications to provide the users with a good experience.

4.4 Circuit boards and connection

The connection of heterogeneous electronic components is significant in textile devices. Electronic textiles that incorporate electronics in textile substrates are 3D, soft, and extensible (3−55% strain) for direct contact with the human body. Therefore, stretchable and flexible circuit boards are required to withstand large, repeated deformation in bending, shear, and tension modes in all directions. Circuit boards provide mechanical support for components and an electrical connection between the components and conductive tracks or pads of a substrate. The circuit boards for textile electronics must be flexible, comfortable, robust, and stretchable. Thus, our review discusses flexible circuit boards that are polyimide (PI) film-, fabric-, and paper-based.

PI materials are commonly used in flexible circuit boards owing to their lightweight properties and high heat and chemical resistance. The fabrication technology of a PI circuit board is similar to the production of rigid print circuit boards (PCBs). A conventional one-sided PI circuit board includes five layers: a base layer of PI (25 μm), layer of adhesive (25 μm), layer of copper (35 μm), second layer of adhesive (20 μm), and PI cover layer (25 μm). The total standard thickness of a multilayer PI circuit board is 130 μm.[208] A developed fabrication technology results in a track width of approximately 75 μm. Another advantage of the PI circuit board is its compatibility with PCB assembly equipment, such as screen printing and surface mount devices. Commercial miniature components can be mounted on a PI circuit board. Sekitani et al. fabricated flexible and conformable organic transistors on PI substrates.[209] The transistors were integrated in a thin catheter that can measure the spatial distribution of pressure. The transistors had extreme bending stability even at a radius of 100 μm. This high flexibility was enabled by a very thin PI substrate (12.5 μm). The resulting flexible pressure sensor can be easily integrated in textile electronics owing to its bending stability and flexibility. However, a disadvantage of the PI circuit board is that the low surface roughness of tracks on a copper film is a hindrance for connecting textile devices and tracks. The multilayer structure leads to an increase in the thickness and limit flexibility, which is another drawback.

Using paper as a substrate for fabricating flexible electronics is another alternative method.[210] The unique porous structure of paper enables the easy absorption of

functional materials for fabricating two-layered paper electronics. Most conductive nanomaterials used for the fabrication of flexible circuits are nonmetallic. The electroconductivity of these materials, such as PEDOT:PSS (8.25×10^3 Sm^{-1}), CNT (5.03×10^3 Sm^{-1}), and carbon (1.8×10^3 Sm^{-1}), is less than that of pure metal materials.[211] Recently, gallium-based liquid metals (LMs) have been utilized to fabricate flexible circuits on paper.[212] Taking advantage of their excellent electrical conductivity (eutectic gallium-indium: 3.4×10^6 Sm^{-1}) and high fluidity, the LMs have been used in flexible electronics, such as pressure sensors,[213] stretchable electromagnetic actuators,[214] and loudspeakers.[215] Guo et al. investigated a paper-based circuit using a one-step LM transfer printing approach.[212b] There are various printing methods, for example, screen printing, gravure printing,[216] offset printing,[217] inkjet printing,[218] flexographic printing,[219] evaporation or vapor deposition,[208] evaporation/sputter deposition/spray-deposition stencil,[208] and brushing and drawing.[220] A paper circuit was used to fabricate a paper umbrella **(Figure 9c)**.[221] The LED lights on the paper circuit were maintained under ideal conditions in the folding and expansion paper umbrella states. Paper electronics can be incorporated in textile electronics owing to their excellent performance, such as flexibility, tailorability, and biodegradability.[222] Liao et al. reported that paper electronics can minimize electronic waste to produce wearable and green electronics.[223] Although paper circuits can work under bending and folding conditions, most paper circuits are suitable for LEDs and cannot be used to embed multi-electronic components.

Electronic circuits can be fabricated by integrating conducted fibers and yarns in a textile by weaving, knitting, embroidery, and stitching processes. Tao el at. developed fabric circuit boards (FCBs) with highly stretchable, three-dimensionally deformable, washable, and durable properties, which are ideal for wearable electronics **(Figure 9d)**.[224] Strain sensors with two soft electrodes were electrically and physically connected using looped conductive fibers for the transmission of electrical signals. The composition of an elastic FCB **(Figure 9e)** and discrete fabric temperature sensors has been utilized to demonstrate the full fabric-based temperature sensor network by Li et al.[225] A challenge for developing knitted and woven FCBs is that the conductive wiring layout should be precisely controlled using a computerized machine. Another challenge is that the conductive fibers and yarns demonstrate high stretchability, which causes performance degradation. Embroidery offers a flexible method to embed conductive yarns on textiles to develop FCBs without damaging the properties of the yarn. Ma et al. developed an inductance–capacitance–resistance (LCR) resonator circuit by sewing a fiber inductor coin in a cotton fabric substrate.[189] The sewed fabric circuit was used to connect a humidity sensor in series, as shown in **Figure 9f**. Although embroidery is less complicated than weaving and knitting in the development of electronic circuits, the conductive traces embedded on the surface of fabrics may trigger short circuits. Conductive fibers or yarns were also utilized in electric textile connections.[226] However, the basic properties of these connections have not been systematically studied; for example, the reliability and wearability of such wire networks when they have numerous connections with rigid electronic components.

4.5 Display hardware

Computers can generate real-time and realistic displays of virtual images, which is a standard VR/AR feature.[9] Existing textile displays are limited in single devices and cannot be used as an alternative immersive display device. The existing display hardware used in VR/AR systems can be divided into desktop, project, and immersive VR/AR according to the degree of immersion that can be attained. Desktop VR/AR is

the simplest display hardware that combines a desktop-based display device, stereoscopic rendering, and head tracking. In VR/AR, a virtual world is viewed through a screen or another display device. Projective VR/AR is an extension of a desktop system and has an enlarged display area. Although the widened view increases the sense of immersion, projective VR/AR is not a truly immersive VR/AR. Immersive images aim at displays with clear indication for users inside a virtual world while blocking cues from their surrounding real environments, which is related to the sense of presence, viz., the feeling of being present in the simulated environment. There are two key examples of display hardware: head-mounted displays and cave automatic virtual environment (CAVE)-like setups. A user in the former type displays should wear a head-mounted setup housing small screens in front of the eyes. By detecting and tracking the head movements of the user, the views of the virtual world are updated based on the viewing orientation and position changes. In the latter displays, a user should stay in a small room whose walls can be employed as projection surfaces to display the virtual world via rear-projection. The two immersive technologies are generally known as "true" VR interfaces.

5. Applications of Wearable VR/AR System

With the integration of textile devices, electric interfaces, power supplies, display hardware, and circuit boards, textile-based systems offer a better experience in emerging VR/AR applications with respect to other sensory interactions than audial and visual interactions. Textile devices enable the wearable VR/AR system to be smaller, softer, and more comfortable, which broadens the range of VR/AR applications.[227] For example, wearable VR/AR textile systems have been explored to improve the quality of life of disabled people and can be beneficial for their recovery.

Haptic devices provide an interaction means for disabled people to have the same opportunities as people with no disabilities. One such remarkable application is robotic prosthetics used in tactile feedback. **Figure 10A** shows a user with an amputated lower arm. An epidermal VR device is attached to his residual limb such that he may grasp objects using a prosthetic arm. Sensors on his prosthetic arm can detect an object shape, which is a piece of input information for creating a virtual haptic representation of a shape on the upper arm.[8] In addition, textile VR/AR devices improve the interaction of social media by providing more stimulations to the experience. **Figure 10B** shows users with a flexible VR device. As a signal of strike was perceived in a combat game, the haptic actuation reproduces the impact pattern at the corresponding body parts.[8] Lee et al. presented the use of textile devices for microclimate control and further evaluated the performance of fabricated devices to enhance the immersive feeling of wearable VR.[119] A wearable heat sink was integrated into a finger-motion tracking glove and independently attached to three devices. **Figure 10C** demonstrates the function of in-situ temperature data collection in realized virtual scenarios, where the users can touch objects with different temperatures, such as a cold beer bottle, chilly soft drink bottle, and mug of warm green tea or hot coffee.

Movement tracking is another advantage of a textile VR/AR device. Textile-based posture and gait devices, such as pressure and strain sensors, can be attached to the human body without causing discomfort. A fiber-type pressure sensor was woven into a glove, and the resistance of the sensor changed according to external stimuli.[110] **Figure 11a** demonstrates a glove used as a wearable controller for VR. When different external stimuli were applied to the smart glove, the ratio of the measured resistances to the initial resistance varied with different external forces, as shown in **Figure 11b**.

Figure 11c shows a VR shooting game controlled by a wearable glove integrated with a multimodal sensor. The bullet re-load and zooming on a target were controlled by applying pressure and bending stress on the first joint of the thumb. The shooting action was produced by folding the index finger.[110] Furthermore, Lou et al. developed a sensing textile for measuring human motions, such as elbow, knee, and underarm monitoring.[111] In addition to monitoring large human motions, such as finger bending and foot movement, Yang et al. reported a textile strain sensor for the detection of different subtle human motions, such as facial expressions and pulse monitoring.[228] Zhou et al. fabricated ultrathin, permeable, and stretchable electrodes that can be integrated into a textile touch sensing system.[229] **Figure 11d** shows that the touch system can identify different finger touches, such as a tap and press. A representative application in playing computer games is shown in **Figure 11e**. When pressing different keys on the sensing sleeve, the Tetris in the game generated different responses, such as rotation, left, right, and down, without a noticeable delay.[229] Patients with Parkinson's disease who wear a VR/AR system can facilitate a normal gait pattern because the virtual image or information can be used as stimuli for therapeutic exercises. In future, VR/AR devices may improve the usage of artificial body parts, as VR/AR can provide body ownership illusion and agency to the users who may conceive that the artificial body part is an actual part of his/her body, and the movement is controlled by himself/herself.

Mental health issues are related to the environment. By employing VR/AR and computer-generated interactive environments, users can experience problematic situations and be educated repeatedly. Through evidence-based psychological treatments, they are encouraged to overcome difficulties.[230] VR/AR can be launched with different set-ups, display devices, and interaction metaphors and paradigms for mental health and related diseases, such as autism spectrum disorders,[231] phantom limb pain,[232] phobia,[233] anxiety disorder,[234] schizophrenia,[235] anorexia and bulimia nervosa,[236] cognitive disabilities,[237] and Parkinson's disease.[238] Freeman el at.[230a] summarized the potential applications of VR in the field of mental health, such as anxiety, depression, psychosis, substance disorder, and eating disorders. The results indicated that the major disorders researched were schizophrenia and anxiety. In addition, exposure-based VR treatments can effectively decrease anxiety disorders. Man et al.[239] adopted a VR prospective memory test to detect the cognitive development of first-episode schizophrenia, which showed that the VR method achieved a 92.9% sensitive and 75% specific measure of prospective memory deficits. VR systems offer a type of reflection and simulation of reality and allow users to be immersed in virtual/artificial environments. Users may perceive that they are performing activities in real-time and feel a sense of satisfaction. Regular VR exercises significantly reduce stress among older adults and improve their sleep quality.[240] More importantly, these VR/AR experiences are a "safe environment" with different simple and complex situations. In addition, these scenarios can be easily recreated manually. However, owing to the complexity of VR/AR systems, there is a lack of wearable, lightweight, and easily handled devices, particularly for the elderly.

The elderly population (>60 years of age) is increasing worldwide.[241] Aging is accompanied by deterioration in functional capacities, sensory sensitivity, and muscular strength,[242] which affects their willingness to participate in daily physical activity.[243] Decline in physical functionalities significantly affects their quality of life. The occurrence of gait impairments and falls become ubiquitous among seniors and people with common neurological diseases.[244] Apart from gait impairment, fear of

cautions gait, falling, dysrhythmicity of stepping, or gait unsteadiness were considered as triggers of fall risk.[245] Thus, attributed to motor and cognitive deficits, fall risk is largely impacted by mental health. Cultivating a habit with regular physical activity is crucial for good mental and physical health. Mak el at.[246] systematically studied the effects of exercises or training on gait, falls, and balance ability in patients with Parkinson's disease and showed that exercise or training can potentially reduce injurious fall risk and lower balance-related fall risks among patients with Parkinson's disease (PD). Moreover, they further explored the longitudinal impact of physical therapy and exercises for patients with PD and showed that sustained dance, aerobic/strength training, or tai chi therapy lasting more than 12 weeks can generate long-term positive effects.[247] VR can allow PD patients to immerse themselves in virtual environments, creating illusions of being present in the non-existent virtual environments. This technology allows people to feel that they perform everything in real-time, which strengthens their enthusiasm for participating in regular physical activities.[238] For example, multi-modal interventions integrating treadmill training with VR can increase the willingness to engage in physical activity and reduce fall risk in PD subjects.[244c]

6. Conclusion

This paper presents a systematic and critical overview and review of the state-of-the-art textile electronics and their applications in VR/AR systems. We discussed the definition, classification, and functions of textile electronics and their integration in VR/AR. Various textile electronic devices, including strain sensors, pressure sensors, connectors, and dry bio-potential electrodes have been developed and have attained technological maturity with good electronic performance, additional flexibility, light weight, and stretchability. Several other textile electronic devices are under extensive investigation in laboratories.[248] However, in the foreseen future, VR/AR systems cannot be completely fabricated in textile structures owing to the limitations of current textile electronic technologies, such as audial and visual interfaces, analog/digital converters, wireless communication modules, memory, data acquisition, and processors. Therefore, heterogeneous integration of rigid microelectronic components with textiles is essential for a complete VR/AR system.

This study has further explored the utilization of textile electronic devices in VR/AR systems. For example, (1) actuators are applied to provide haptic action, (2) pressure and strain sensors used to monitor human motions, such as posture and gait, (3) heating and cooling textile devices used to control microclimate surrounding the human body, and (4) textile electrodes employed to measure biopotential signals, and detect and analyze brain activity. Appropriate selection of textile electronic devices, electronic interfaces, energy supply, and flexible circuit boards can yield significant improvements in the immersion and portable performance of VR/AR. Numerous potential applications have been discussed for textile electronics in VR/AR, such as tactile feedback, interaction of social media, tracking, microclimate control, and human mental health. Although VR/AR systems cannot be completely fabricated in textile structures, we believe that adopting certain developed textile electronic devices can provide further user-friendly immersing VR/AR experiences.

Major hindrances to the progress of textile electronic VR/AR systems are insufficient performance, immature production technology, and lack of system-level investigations and standards. The general lifetime of textile electronics is shorter than that of rigid microelectronic devices. For example, conductive materials on textiles can be easily

detached or damaged due to mechanical motion during wear and corrosion.[249] Many textile electronics produced from organic or polymer functional materials are sensitive to water and oxygen, and the laundering process of textiles can cause deterioration of function. Moreover, most textile electronics experiments were conducted in the laboratory-scale or research stage, and very few textile electronics were commercialized because many devices were made using manual techniques instead of machinery. The large-scale manufacturability and reproducibility of textile electronics are uncertain. Further, current research generally focuses on materials or single devices or demonstration applications, and there has been limited research on the system integration of textile electronics. A system requires the cooperation and connection of different modules to realize complicated analyses and functions. The divergence of materials, structures, and fabrication techniques used in textile electronics devices can cause conflict between devices and restrict their applications. System-level investigations may identify and address these problems. Furthermore, the absence of calibration systems and standards hinders the industrialization and commercialization of textile electronics.

Acknowledgements

This work was partially supported by Research Grants Council (No. 15211016E, 15200917E, 15201419E), Innovation and Technology Commission (No. ITS/306/17) of the Hong Kong SAR Government, China, and Hong Kong Polytechnic University (No. AAB3 and 847A). Postgraduate scholarships received from Hong Kong Polytechnic University are appreciated by Liu and Ma. The TOC artistic description was provided by Naomi X.J. Ding.

References:

[1] J. Lanier, *Scientific American* **2001**, 284, 66.

[2] P. Fuchs, G. Moreau, P. Guitton, *Virtual reality: concepts and technologies*, CRC Press, **2011**.

[3] R. T. Azuma, *Presence: Teleoperators & Virtual Environments* **1997**, 6, 355.

[4] J. Peddie, *Augmented reality: Where we will all live*, Springer, **2017**.

[5] D. Schmalstieg, T. Hollerer, *Augmented reality: principles and practice*, Addison-Wesley Professional, **2016**.

[6] J. Shi, S. Liu, L. Zhang, B. Yang, L. Shu, Y. Yang, M. Ren, Y. Wang, J. Chen, W. Chen, Y. Chai, X. Tao, *Adv Mater* **2020**, 32, 1901958.

[7] X. Tao, *Smart fibres, fabrics and clothing: fundamentals and applications*, Elsevier, **2001**.

[8] X. Yu, Z. Xie, Y. Yu, J. Lee, A. Vazquez-Guardado, H. Luan, J. Ruban, X. Ning, A. Akhtar, D. Li, Ji Bowen, Liu Yiming, Sun Rujie, Cao Jingyue, Huo Qingze, Zhong Yishan, Lee ChanMi, Kim SeungYeop, Gutruf Philipp, Zhang Changxing, Xue Yeguang, Guo Qinglei, Chempakasseril Aditya, Tian Peilin, Lu Wei, Jeong JiYoon, Yu YongJoon, Cornman Jesse, Tan CheeSim, Kim BongHoon, Lee KunHyuk, Feng Xue, Huang Yonggang, R. J. A., *Nature* **2019**, 575, 473.

[9] B. Furht, *Handbook of augmented reality*, Springer Science & Business Media, **2011**.

[10] C. Cork, in *Electronic Textiles*, Elsevier **2015**, p. 3.

[11] D. Meoli, T. J. J. o. T. May-Plumlee, T. Apparel, Management, **2002**, 2, 1.

[12] D. A. Hardy, I. Anastasopoulos, M.-N. Nashed, C. Oliveira, T. Hughes-Riley, A. Komolafe, J. Tudor, R. Torah, S. Beeby, T. Dias, *Microsyst Technol* **2019**, 1.

[13] A. Bedeloglu, N. Sunter, Y. J. M. Bozkurt, M. Processes, **2011**, 26, 1378.

[14] T. Y. Choi, B. U. Hwang, B. Y. Kim, T. Q. Trung, Y. H. Nam, D. N. Kim, K. Eom, N. E. Lee, *ACS Appl Mater Interfaces* **2017**, 9, 18022.

[15] D. Huo, M. J. Kim, Z. Lyu, Y. Shi, B. J. Wiley, Y. J. C. r. Xia, **2019**, 119, 8972.

[16] J. Song, *Smart Textiles: Wearable Nanotechnology* **2018**, 127.

[17] F. Xu, Y. Zhu, *Adv Mater* **2012**, 24, 5117.

[18] P. Lee, J. Lee, H. Lee, J. Yeo, S. Hong, K. H. Nam, D. Lee, S. S. Lee, S. H. Ko, *Adv Mater* **2012**, 24, 3326.

[19] T. An, S. Gong, Y. Ling, D. Dong, Y. Zhao, W. Cheng, *EcoMat* **2020**.

[20] T. Sannicolo, M. Lagrange, A. Cabos, C. Celle, J. P. Simonato, D. Bellet, *Small* **2016**, 12, 6052.

[21] A. M. Grancarić, I. Jerković, V. Koncar, C. Cochrane, F. M. Kelly, D. Soulat, X. Legrand, *J. Ind. Text.* **2018**, 48, 612.

[22] K. Uh, T. Kim, C. W. Lee, J. M. Kim, *Macromol. Mater. Eng.* **2016**, 301, 1320.

[23] G. B. Tseghai, D. A. Mengistie, B. Malengier, K. A. Fante, L. Van Langenhove, *Sensors (Basel)* **2020**, 20.

[24] Y. Wang, C. Zhu, R. Pfattner, H. Yan, L. Jin, S. Chen, F. Molina-Lopez, F. Lissel, J. Liu, N. I. Rabiah, *Science advances* **2017**, 3, e1602076.

[25] R. Sarabia-Riquelme, M. Shahi, J. W. Brill, M. C. Weisenberger, *ACS Applied Polymer Materials* **2019**, 1, 2157.

[26] D. Yuan, B. Li, J. Cheng, Q. Guan, Z. Wang, W. Ni, C. Li, H. Liu, B. Wang, *J. Mater. Chem. A* **2016**, 4, 11616.

[27] E. Číková, M. Mičušík, A. Šišková, M. Procházka, P. Fedorko, M. Omastová, *Synth Met* **2018**, 235, 80.

[28] a) C. Yu, J. An, R. Zhou, H. Xu, J. Zhou, Q. Chen, G. Sun, W. Huang, *Small* **2020**, 2000653; b) F. Wang, S. Liu, L. Shu, X.-M. Tao, *Carbon* **2017**, 121, 353.

[29] L. Dumas, L. Bonnaud, P. Dubois, in *Advanced and emerging polybenzoxazine science and technology*, Elsevier **2017**, p. 767.

[30] E. Frank, F. Hermanutz, M. R. Buchmeiser, *Macromolecular Materials and Engineering* **2012**, 297, 493.
[31] H.-S. Kil, K. Oh, Y.-J. Kim, S. Ko, Y. P. Jeon, H.-I. Joh, Y.-K. Kim, S. Lee, *Journal of Analytical and Applied Pyrolysis* **2018**, 136, 153.
[32] J. Di, X. Zhang, Z. Yong, Y. Zhang, D. Li, R. Li, Q. Li, *Advanced materials* **2016**, 28, 10529.
[33] M. Zhang, K. R. Atkinson, R. H. Baughman, *Science* **2004**, 306, 1358.
[34] X. Zhang, Q. Li, Y. Tu, Y. Li, J. Y. Coulter, L. Zheng, Y. Zhao, Q. Jia, D. E. Peterson, Y. Zhu, *small* **2007**, 3, 244.
[35] H. Zhao, Y. Zhang, P. D. Bradford, Q. Zhou, Q. Jia, F.-G. Yuan, Y. Zhu, *Nanotechnology* **2010**, 21, 305502.
[36] Z. Dong, C. Jiang, H. Cheng, Y. Zhao, G. Shi, L. Jiang, L. Qu, *Advanced Materials* **2012**, 24, 1856.
[37] J. Kim, J. W. Kim, H. C. Kim, L. Zhai, H.-U. Ko, R. M. Muthoka, *Int J Precis Eng Man* **2019**, 1.
[38] W. Jayathilaka, K. Qi, Y. Qin, A. Chinnappan, W. Serrano-Garcia, C. Baskar, H. Wang, J. He, S. Cui, S. W. Thomas, S. Ramakrishna, *Adv Mater* **2019**, 31, e1805921.
[39] S. M. Mirvakili, I. W. Hunter, *Adv Mater* **2018**, 30, 1704407.
[40] D. Melling, J. G. Martinez, E. W. H. Jager, *Adv Mater* **2019**, 31, e1808210.
[41] D. P. Karothu, J. Mahmoud Halabi, L. Li, A. Colin‐Molina, B. Rodríguez‐Molina, P. Naumov, *Adv Mater* **2020**, 32, 1906216.
[42] Y. Song, S. Zhou, K. Jin, J. Qiao, D. Li, C. Xu, D. Hu, J. Di, M. Li, Z. Zhang, L. Qingwen, *Nanoscale* **2018**, 10, 4077.
[43] E. W. H. Jager, J. G. Martinez, Y. Zhong, N.-K. Persson, in *Wearable Bioelectronics*, DOI: 10.1016/b978-0-08-102407-2.00008-4 **2020**, p. 201.
[44] R. Yin, B. Yang, X. Ding, S. Liu, W. Zeng, J. Li, S. Yang, X. Tao, *Advanced Materials Technologies* **2020**, 5, 2000341.
[45] D. Kongahage, J. Foroughi, *Fibers* **2019**, 7, 21.
[46] S. Shian, K. Bertoldi, D. R. Clarke, *Adv Mater* **2015**, 27, 6814.
[47] Y. Wu, Y. Yang, C. Li, Y. Li, W. Chen, *Frontiers in bioengineering and biotechnology* **2020**, 8.
[48] L. Cappello, K. C. Galloway, S. Sanan, D. A. Wagner, R. Granberry, S. Engelhardt, F. L. Haufe, J. D. Peisner, C. J. Walsh, *Soft Robot* **2018**, 5, 662.
[49] a) Y. Li, Y. Li, M. Su, W. Li, Y. Li, H. Li, X. Qian, X. Zhang, F. Li, Y. Song, *Advanced Electronic Materials* **2017**, 3; b) C. Wang, X. Li, E. Gao, M. Jian, K. Xia, Q. Wang, Z. Xu, T. Ren, Y. Zhang, *Adv Mater* **2016**, 28, 6640.
[50] Y. Huang, L. Gao, Y. Zhao, X. Guo, C. Liu, P. Liu, *J. Appl. Polym. Sci.* **2017**, 134, 45340.
[51] S. Seyedin, P. Zhang, M. Naebe, S. Qin, J. Chen, X. Wang, J. M. Razal, *Materials Horizons* **2019**, 6, 219.
[52] J. Lee, S. Shin, S. Lee, J. Song, S. Kang, H. Han, S. Kim, S. Kim, J. Seo, D. Kim, *ACS Nano* **2018**, 12, 4259.
[53] G. Cai, M. Yang, Z. Xu, J. Liu, B. Tang, X. Wang, *Chemical Engineering Journal* **2017**, 325, 396.
[54] S. J. Lim, J. H. Bae, J. H. Han, S. J. Jang, H. J. Oh, W. Lee, S. H. Kim, J. H. Ko, *Smart Mater Struct* **2020**, 29, 055010.
[55] O. Atalay, A. Atalay, J. Gafford, C. Walsh, *Advanced materials technologies* **2018**, 3, 1700237.
[56] A. Elsayes, V. Sharma, K. Yiannacou, A. Koivikko, A. Rasheed, V. Sariola, *Advanced Sustainable Systems* **2020**, 2000056.
[57] K. Qi, H. Wang, X. You, X. Tao, M. Li, Y. Zhou, Y. Zhang, J. He, W. Shao, S. Cui, *J. Colloid Interface Sci.* **2020**, 561, 93.
[58] C. Garcia, I. Trendafilova, R. G. de Villoria, J. S. del Rio, *Nano Energy* **2018**, 50, 401.

[59] J. Xu, G. Wang, Y. Wu, X. Ren, G. Gao, *ACS applied materials & interfaces* **2019**, 11, 25613.
[60] E. S. Hosseini, L. Manjakkal, D. Shakthivel, R. Dahiya, *ACS applied materials & interfaces* **2020**, 12, 9008.
[61] M. Husain, R. Kennon, *Fibers* **2013**, 1, 2.
[62] Q. Li, L. N. Zhang, X. M. Tao, X. Ding, *Adv Healthc Mater* **2017**, 6, 1601371.
[63] M. D. Husain, R. Kennon, *Fibers* **2013**, 1, 2.
[64] Z. Cui, F. R. Poblete, Y. Zhu, *ACS applied materials & interfaces* **2019**, 11, 17836.
[65] F. Wang, J. Jiang, F. Sun, L. Sun, T. Wang, Y. Liu, M. Li, *Cellulose* **2019**, 27, 2369.
[66] T. Q. Trung, H. S. Le, T. M. L. Dang, S. Ju, S. Y. Park, N. E. Lee, *Adv Healthc Mater* **2018**, 7, 1800074.
[67] S. H. Lim, L. Feng, J. W. Kemling, C. J. Musto, K. S. Suslick, *Nature chemistry* **2009**, 1, 562.
[68] R. E. Owyeung, M. J. Panzer, S. R. Sonkusale, *Sci. Rep.* **2019**, 9, 1.
[69] Y. J. Yun, W. G. Hong, H. J. Kim, Y. Jun, H.-K. Lee, *Sensors and Actuators B: Chemical* **2017**, 248, 829.
[70] Y. Zhang, J. Zhao, T. Du, Z. Zhu, J. Zhang, Q. Liu, *Sci. Rep.* **2017**, 7, 1.
[71] S. Yao, J. Yang, F. R. Poblete, X. Hu, Y. Zhu, *ACS applied materials & interfaces* **2019**, 11, 31028.
[72] A. Kapoor, M. McKnight, K. Chatterjee, T. Agcayazi, H. Kausche, A. Bozkurt, T. K. Ghosh, *Advanced Materials Technologies* **2019**, 4, 1800281.
[73] M. Zohair, K. Moyer, J. Eaves-Rathert, C. Meng, J. Waugh, C. L. Pint, *ACS Nano* **2020**, 14, 2308.
[74] R. R. Rajanna, N. Sriraam, P. R. Vittal, U. Arun, *IEEE Sensors J.* **2020**, 20, 1573.
[75] R. A. Munteanu, S. Banuleasa, A. Rusu, D. G. Butacu, *Advances in Electrical and Computer Engineering* **2020**, 20, 73.
[76] W. Q. Wu, S. Pirbhulal, A. K. Sangaiah, S. C. Mukhopadhyay, G. L. Li, *Future Gener Comp Sy* **2018**, 86, 515.
[77] L. Shu, T. Y. Xu, X. M. Xu, *IEEE Sensors J.* **2019**, 19, 5995.
[78] a) M. A. Shathi, M. Z. Chen, N. A. Khoso, H. Deb, A. Ahmed, W. S. Sai, *Synth Met* **2020**, 263, 116329; b) D. Pani, A. Achilli, A. Spanu, A. Bonfiglio, M. Gazzoni, A. Botter, *Ieee T Neur Sys Reh* **2019**, 27, 1370.
[79] N. N. Zhang, L. N. Yue, Y. J. Xie, O. W. Samuel, O. M. Omisore, W. H. Pei, X. Xing, C. Lin, Y. D. Zheng, L. Wang, *Ieee J Transl Eng He* **2018**, 6, 1.
[80] D. Pani, A. Achilli, A. Bonfiglio, *Advanced Materials Technologies* **2018**, 3, 1800008.
[81] A. Ankhili, S. U. Zaman, X. Tao, C. Cochrane, V. Koncar, D. Coulon, *IEEE Sensors J.* **2019**, 19, 11995.
[82] K. Arquilla, A. K. Webb, A. P. Anderson, *Sensors* **2020**, 20, 1013.
[83] E. Bihar, T. Roberts, E. Ismailova, M. Saadaoui, M. Isik, A. Sanchez‐Sanchez, D. Mecerreyes, T. Hervé, J. B. De Graaf, G. G. Malliaras, *Advanced Materials Technologies* **2017**, 2, 1600251.
[84] S. Takamatsu, T. Lonjaret, D. Crisp, J.-M. Badier, G. G. Malliaras, E. Ismailova, *Sci. Rep.* **2015**, 5, 15003.
[85] G. Li, S. Wang, Y. Y. Duan, *Sensors and Actuators B: Chemical* **2017**, 241, 1244.
[86] K. Takagahara, K. Ono, N. Oda, T. Teshigawara, *NTT Technical Review* **2014**, 12, 1.
[87] G. Paul, R. Torah, S. Beeby, J. Tudor, *Sensors and Actuators A: Physical* **2014**, 206, 35.
[88] M. Inoue, Y. Amano, Y. Tada, presented at 2017 International Conference on Electronics Packaging (ICEP) **2017**.
[89] T. Takeshita, M. Yoshida, Y. Takei, A. Ouchi, A. Hinoki, H. Uchida, T. Kobayashi, *Sci. Rep.* **2019**, 9, 1.
[90] C. J. Wilson, A. Soranzo, *Comput Math Method M* **2015**, DOI: 10.1155/2015/151702.

[91] M. Hoppe, P. Knierim, T. Kosch, M. Funk, L. Futami, S. Schneegass, N. Henze, A. Schmidt, T. Machulla, presented at Proceedings of the 17th International Conference on Mobile and Ubiquitous Multimedia **2018**.
[92] D. X. Wang, K. Ohnishi, W. L. Xu, *Ieee T Ind Electron* **2020**, 67, 610.
[93] C. Pacchierotti, S. Sinclair, M. Solazzi, A. Frisoli, V. Hayward, D. Prattichizzo, *Ieee T Haptics* **2017**, 10, 580.
[94] M. Bianchi, E. Battaglia, M. Poggiani, S. Ciotti, A. Bicchi, presented at 2016 IEEE haptics symposium (HAPTICS) **2016**.
[95] Y. Lee, M. Kim, Y. Lee, J. Kwon, Y. L. Park, D. Lee, *Ieee-Asme T Mech* **2019**, 24, 67.
[96] a) S. Casini, M. Morvidoni, M. Bianchi, M. Catalano, G. Grioli, A. Bicchi, presented at Ieee Int C Int Robot **2015**; b) J. J. Huaroto, E. Suarez, H. I. Krebs, P. D. Marasco, E. A. Vela, *Ieee Robotics and Automation Letters* **2019**, 4, 17.
[97] H. Kim, C. Seo, J. Lee, J. Ryu, S.-b. Yu, S. Lee, presented at 2006 IEEE Intelligent Transportation Systems Conference **2006**.
[98] S. Cao, X. Li, X. Yan, D. Jiang, Q. Guo, presented at 2018 IEEE 4th Information Technology and Mechatronics Engineering Conference (ITOEC) **2018**.
[99] W. H. Park, E. J. Shin, Y. Yoo, S. Choi, S. Y. Kim, *Ieee T Ind Electron* **2020**, 67, 677.
[100] Z. Zhang, B. Zhu, Z. Peng, R. Yin, R. H. Baughman, X. Tao, *Advanced Materials Technologies* **2020**, 2000329.
[101] C. W. Carpenter, S. T. M. Tan, C. Keef, K. Skelil, M. Malinao, D. Rodriquez, M. A. Alkhadra, J. Ramirez, D. J. Lipomi, *Sensor Actuat a-Phys* **2019**, 288, 79.
[102] G. Chernyshov, B. Tag, C. Caremel, F. Cao, G. Liu, K. Z. Kai, Acm, *Shape Memory Alloy Wire Actuators for Soft, Wearable Haptic Devices*, **2018**.
[103] W. Fang, L. Zheng, X. Wu, *Comput Ind* **2017**, 92, 91.
[104] F. Zhou, H. B. L. Duh, M. Billinghurst, in *7th Ieee International Symposium on Mixed and Augmented Reality 2008, Proceedings* (Eds: M. A. Livingston, O. Bimber, H. Saito) **2008**, p. 193.
[105] M. Sudha, K. Sriraghav, S. G. Jacob, S. Manisha, *International Journal of Ambient Computing and Intelligence (IJACI)* **2017**, 8, 1.
[106] A. Muro-de-la-Herran, B. Garcia-Zapirain, A. Mendez-Zorrilla, *Sensors* **2014**, 14, 3362.
[107] L. Shu, X. M. Tao, D. D. Feng, *IEEE Sensors J.* **2015**, 15, 442.
[108] W. J. Tao, T. Liu, R. C. Zheng, H. T. Feng, *Sensors* **2012**, 12, 2255.
[109] a) S. T. Yang, C. W. Li, X. Y. Chen, Y. P. Zhao, H. Zhang, N. X. Wen, Z. Fan, L. J. Pan, *Acs Applied Materials & Interfaces* **2020**, 12, 19874; b) Z. H. Ma, W. Wang, D. Yu, *Energy Technology* **2020**, DOI: 10.1002/ente.202000164; c) Y. Sun, Z. Du, *Nanomaterials* **2019**, 9, 945.
[110] S. Choi, K. Yoon, S. Lee, H. J. Lee, J. Lee, D. W. Kim, M. S. Kim, T. Lee, C. Pang, *Adv. Funct. Mater.* **2019**, 29, 1905808.
[111] M. N. Lou, I. Abdalla, M. M. Zhu, X. D. Wei, J. Y. Yu, Z. L. Li, B. Ding, *Acs Applied Materials & Interfaces* **2020**, 12, 19965.
[112] S. Yao, Y. Zhu, *Nanoscale* **2014**, 6, 2345.
[113] C. Wang, Y. Kim, H. Shin, S. D. Min, *Sensors* **2019**, 19, 3950.
[114] a) M. N. Lou, I. Abdalla, M. M. Zhu, J. Y. Yu, Z. L. Li, B. Ding, *Acs Applied Materials & Interfaces* **2020**, 12, 1597; b) T. He, Z. Sun, Q. Shi, M. Zhu, D. V. Anaya, M. Xu, T. Chen, M. R. Yuce, A. V.-Y. Thean, C. Lee, *Nano Energy* **2019**, 58, 641; c) H. X. Wu, H. Guo, Z. M. Su, M. Y. Shi, X. X. Chen, X. L. Cheng, M. D. Han, H. X. Zhang, *J. Mater. Chem. A* **2018**, 6, 20277.
[115] F. Wen, Z. D. Sun, T. Y. Y. He, Q. F. Shi, M. L. Zhu, Z. X. Zhang, L. H. Li, T. Zhang, C. K. Lee, *Adv Sci* **2020**, 7, 2000261.
[116] S. Sundaram, P. Kellnhofer, Y. Li, J.-Y. Zhu, A. Torralba, W. Matusik, *Nature* **2019**, 569, 698.

[117] a) C. C. Vu, J. Kim, *Sensors* **2018**, 18, 3109; b) C. Vu, J. Kim, *Fibers Polym.* **2018**, 19, 2657.
[118] J. S. Roh, S. Kim, *J Intel Mat Syst Str* **2016**, 27, 1165.
[119] J. Lee, H. Sul, W. Lee, K. R. Pyun, I. Ha, D. Kim, H. Park, H. Eom, Y. Yoon, J. Jung, *Adv. Funct. Mater.* **2020**, 30, 1909171.
[120] J. Tabor, K. Chatterjee, T. K. Ghosh, *Advanced Materials Technologies* **2020**, 5.
[121] H.-J. Hwang, H. Devaraj, C. Yang, Z. Gao, C.-h. Chang, H. Lee, R. Malhotra, *Sci. Rep.* **2018**, 8, 1.
[122] a) J. N. Huang, Y. R. Li, Z. J. Xu, W. F. Li, B. B. Xu, H. Q. Meng, X. Y. Liu, W. X. Guo, *Nanotechnology* **2019**, 30, 325203; b) Y. Cheng, H. Zhang, R. Wang, X. Wang, H. Zhai, T. Wang, Q. Jin, J. Sun, *ACS Applied Materials & Interfaces* **2016**, 8, 32925.
[123] K. L. Qiu, A. Elhassan, T. H. Tian, X. Yin, J. Y. Yu, Z. L. Li, B. Ding, *Acs Applied Materials & Interfaces* **2020**, 12, 11016.
[124] a) S. Liu, J. Tong, C. Yang, L. Li, *Text. Res. J.* **2017**, 87, 1669; b) S. Liu, C. Yang, Y. Zhao, X. m. Tao, J. Tong, L. Li, *Text. Res. J.* **2016**, 86, 1455; c) S. Liu, *The Hong Kong Polytechnic Unversity* **2017**.
[125] H. Zhang, X. Tao, T. Yu, S. Wang, *Sensors and Actuators A: Physical* **2006**, 126, 129.
[126] P. Liu, Y. Li, Y. Xu, L. Bao, L. Wang, J. Pan, Z. Zhang, X. Sun, H. Peng, *Small* **2018**, 14, 1702926.
[127] H. Kim, S. Lee, *Polymers* **2019**, 11, 928.
[128] a) H. Luo, Q. Li, K. K. Du, Z. Q. Xu, H. Z. Zhu, D. L. Liu, L. Cai, P. Ghosh, M. Qiu, *Nano Energy* **2019**, 65; b) Q. W. Wang, H. B. Zhang, J. Liu, S. Zhao, X. Xie, L. X. Liu, R. Yang, N. Koratkar, Z. Z. Yu, *Adv. Funct. Mater.* **2019**, 29; c) L. S. Zhang, M. Baima, T. L. Andrew, *Acs Applied Materials & Interfaces* **2017**, 9, 32299; d) C. Yeon, G. Kim, J. Lim, S. Yun, *RSC Adv.* **2017**, 7, 5888; e) P. Ilanchezhiyan, A. Zakirov, G. M. Kumar, S. U. Yuldashev, H. Cho, T. Kang, A. Mamadalimov, *RSC Adv.* **2015**, 5, 10697.
[129] a) P. Kotagama, A. Phadnis, K. C. Manning, K. Rykaczewski, *Advanced Materials Technologies* **2019**, 4, 1800690; b) S. Hong, Y. Gu, J. K. Seo, J. Wang, P. Liu, Y. S. Meng, S. Xu, R. Chen, *Science advances* **2019**, 5, eaaw0536.
[130] R. Riener, M. Harders, *Virtual reality in medicine*, Springer Science & Business Media, **2012**.
[131] T. Narumi, T. Kajinami, S. Nishizaka, T. Tanikawa, M. Hirose, presented at 2011 IEEE Virtual Reality Conference **2011**.
[132] X. Hu, K. Tong, X. Wei, W. Rong, E. A. Susanto, S.-K. Ho, presented at 2013 35th Annual International Conference of the IEEE Engineering in Medicine and Biology Society (EMBC) **2013**.
[133] M. Wawrzyk, K. Wesolowska, M. Plechawska-Wojcik, T. Szymczyk, in *Information Systems Architecture and Technology, Isat 2018, Pt I*, Vol. 852 (Eds: L. Borzemski, J. Swiatek, Z. Wilimowska) **2019**, p. 222.
[134] L. M. Vortmann, F. Kroll, F. Putze, *Front Hum Neurosci* **2019**, 13, 348.
[135] X. Li, Y. Sun, presented at 2017 IEEE EMBS International Conference on Biomedical & Health Informatics (BHI) **2017**.
[136] M. C. Garcia, T. Vieira, *Revista andaluza de medicina del deporte* **2011**, 4, 17.
[137] a) H. Türker, H. Sze, *Electrodiagnosis in new frontiers of clinical research* **2013**, 175; b) M. R. Al-Mulla, F. Sepulveda, M. Colley, *Sensors* **2011**, 11, 3545.
[138] G. Acar, O. Ozturk, A. J. Golparvar, T. A. Elboshra, K. Böhringer, M. K. Yapici, *Electronics-Switz* **2019**, 8, 479.
[139] E. J. Pino, Y. Arias, P. Aqueveque, presented at 2018 40th Annual International Conference of the IEEE Engineering in Medicine and Biology Society (EMBC) **2018**.
[140] A. Shafti, R. B. R. Manero, A. M. Borg, K. Althoefer, M. J. Howard, *Ieee T Neur Sys Reh* **2016**, 25, 1472.

[141] O. Tikkanen, S. KäRKKäINEN, P. Haakana, M. Kallinen, T. Pullinen, T. Finni, *Medicine & Science in Sports & Exercise* **2014**, 46, 1831.
[142] R. Zhang, S. Bernhart, O. Amft, presented at 2016 IEEE 13th International Conference on Wearable and Implantable Body Sensor Networks (BSN) **2016**.
[143] S. Hertweck, D. Weber, H. Alwanni, F. Unruh, M. Fischbach, M. E. Latoschik, T. Ball, Ieee, *Brain Activity in Virtual Reality: Assessing Signal Quality of High-Resolution EEG While Using Head-Mounted Displays*, **2019**.
[144] F. Lotte, J. Faller, C. Guger, Y. Renard, G. Pfurtscheller, A. Lécuyer, R. Leeb, in *Towards Practical Brain-Computer Interfaces*, Springer **2012**, p. 197.
[145] Q. Gao, M. Wang, X. Kang, C. Zhu, M. Ge, *Composites Communications* **2020**, 17, 134.
[146] S.-W. Kim, S.-N. Kwon, S.-I. Na, *Compos Part B: Eng* **2019**, 167, 573.
[147] P. Pötschke, T. Andres, T. Villmow, S. Pegel, H. Brünig, K. Kobashi, D. Fischer, L. Häussler, *Composites Science and Technology* **2010**, 70, 343.
[148] Y.-C. Huang, T.-Y. Lo, C.-H. Chen, K.-H. Wu, C.-M. Lin, W.-T. Whang, *Sensors and Actuators B: Chemical* **2015**, 216, 603.
[149] K. Low, C. B. Horner, C. Li, G. Ico, W. Bosze, N. V. Myung, J. Nam, *Sensors and Actuators B: Chemical* **2015**, 207, 235.
[150] X. Yang, X. Hu, Q. Wang, J. Xiong, H. Yang, X. Meng, L. Tan, L. Chen, Y. Chen, *ACS Applied Materials & Interfaces* **2017**, 9, 26468.
[151] J. Suikkola, T. Bjorninen, M. Mosallaei, T. Kankkunen, P. Iso-Ketola, L. Ukkonen, J. Vanhala, M. Mantysalo, *Sci Rep* **2016**, 6, 25784.
[152] S.-H. Ke, Q.-W. Xue, C.-Y. Pang, P.-W. Guo, W.-J. Yao, H.-P. Zhu, W. Wu, *Nanomaterials* **2019**, 9, 686.
[153] Y. Mao, M. Zhu, W. Wang, D. Yu, *Soft Matter* **2018**, 14, 1260.
[154] N. Karim, S. Afroj, A. Malandraki, S. Butterworth, C. Beach, M. Rigout, K. S. Novoselov, A. J. Casson, S. G. Yeates, *Journal of Materials Chemistry C* **2017**, 5, 11640.
[155] Z. Stempien, E. Rybicki, T. Rybicki, J. Lesnikowski, *Sensors and Actuators B: Chemical* **2016**, 224, 714.
[156] H. Shahariar, I. Kim, H. Soewardiman, J. S. Jur, *ACS Appl Mater Interfaces* **2019**, 11, 6208.
[157] J.-U. Park, M. Hardy, S. J. Kang, K. Barton, K. Adair, D. k. Mukhopadhyay, C. Y. Lee, M. S. Strano, A. G. Alleyne, J. G. Georgiadis, P. M. Ferreira, J. A. Rogers, *Nat Mater* **2007**, 6, 782.
[158] S. Agarwala, G. L. Goh, T.-S. Dinh Le, J. An, Z. K. Peh, W. Y. Yeong, Y.-J. Kim, *ACS sensors* **2018**, 4, 218.
[159] T. He, Q. Shi, H. Wang, F. Wen, T. Chen, J. Ouyang, C. Lee, *Nano Energy* **2019**, 57, 338.
[160] L. Allison, S. Hoxie, T. L. Andrew, *Chem. Commun.* **2017**, 53, 7182.
[161] C. Anand Subhash, A. R. Horrocks, 2016, 1.
[162] T. A. Khattab, M. Rehan, Y. Hamdy, T. I. Shaheen, *Ind Eng Chem Res* **2018**, 57, 11483.
[163] F. Gong, C. Meng, J. He, X. Dong, *Prog Org Coat* **2018**, 121, 89.
[164] A. Atalay, V. Sanchez, O. Atalay, D. M. Vogt, F. Haufe, R. J. Wood, C. J. Walsh, *Advanced Materials Technologies* **2017**, 2, 1700136.
[165] X.-Q. Tan, J.-Y. Liu, J.-R. Niu, J.-Y. Liu, J.-Y. Tian, *Materials* **2018**, 11, 1953.
[166] Q. Wei, Y. Xu, Y. Wang, in *Surface Modification of Textiles*, DOI: 10.1533/9781845696689.58 **2009**, p. 58.
[167] Q. Wei, Q. Li, D. Hou, Z. Yang, W. Gao, *Surface and Coatings Technology* **2006**, 201, 1821.
[168] S. Jiang, Y. Wang, J. Xu, D. Miao, S. Shang, L. Peng, R. Guo, *Journal of Materials Science: Materials in Electronics* **2017**, 28, 18936.
[169] E. Sacher, *Metallization of polymers 2*, Kluwer Academic/Plenum Publishers, New York **2002**.

[170] A. Yli-Pentti, in *Comprehensive Materials Processing*, DOI: https://doi.org/10.1016/B978-0-08-096532-1.00413-1 (Eds: S. Hashmi, G. F. Batalha, C. J. Van Tyne, B. Yilbas), Elsevier, Oxford **2014**, p. 277.
[171] C. A. Loto, *Silicon* **2016**, 8, 177.
[172] Z. Ma, R. Xu, W. Wang, D. Yu, *Colloids and Surfaces A: Physicochemical and Engineering Aspects* **2019**, 582, 123918.
[173] S. J. Park, T.-J. Ko, J. Yoon, M.-W. Moon, K. H. Oh, J. H. Han, *Applied Surface Science* **2017**, 396, 1678.
[174] R. Guo, S. Jiang, C. Yuen, M. Ng, *Journal of The Textile Institute* **2012**, 103, 1267.
[175] H. Zhao, L. Hou, J. X. Wu, Y. X. Lu, *Journal of Materials Chemistry C* **2016**, 4, 7156.
[176] W. Sha, X. Wu, K. G. Keong, *Electroless copper and nickel-phosphorus plating: processing, characterisation and modelling*, Elsevier, **2011**.
[177] A. Ali, V. Baheti, J. Militky, *Materials Chemistry and Physics* **2019**, 231, 33.
[178] M. Wang, X. Wang, P. Moni, A. Liu, D. H. Kim, W. J. Jo, H. Sojoudi, K. K. Gleason, *Adv Mater* **2017**, 29.
[179] T. Bashir, M. Skrifvars, N. K. Persson, *Polymers for Advanced Technologies* **2011**, 22, 2214.
[180] C. Yao, A. Yuan, H. Zhang, B. Li, J. Liu, F. Xi, X. Dong, *J. Colloid Interface Sci.* **2019**, 533, 144.
[181] J. Lv, P. Zhou, L. Zhang, Y. Zhong, X. Sui, B. Wang, Z. Chen, H. Xu, Z. Mao, *Chemical Engineering Journal* **2019**, 361, 897.
[182] Z. Yue, J. Economy, in *Activated Carbon Fiber and Textiles*, DOI: 10.1016/b978-0-08-100660-3.00004-3 **2017**, p. 61.
[183] Y. Liu, S. Kumar, *Polymer Reviews* **2012**, 52, 234.
[184] J. Zhu, Y. Wu, X. Huang, L. Huang, M. Cao, G. Song, X. Guo, X. Sui, R. Ren, J. Chen, *Nano Energy* **2019**, 62, 883.
[185] Q. Li, J. Wang, C. Liu, S. M. Fakhrhoseini, D. Liu, L. Zhang, W. Lei, M. Naebe, *Advanced Science* **2019**, 6, 1900762.
[186] M. Zhang, C. Wang, H. Wang, M. Jian, X. Hao, Y. Zhang, *Advanced Functional Materials* **2017**, 27, 1604795.
[187] C. Falconi, E. Martinelli, C. Di Natale, A. D'Amico, F. Maloberti, P. Malcovati, A. Baschirotto, V. Stornelli, G. Ferri, *Sensors and Actuators B: Chemical* **2007**, 121, 295.
[188] L. Shu, The Hong Kong Polytechnic University, **2012**.
[189] L. Y. Ma, R. H. Wu, A. Patil, S. H. Zhu, Z. H. Meng, H. Q. Meng, C. Hou, Y. F. Zhang, Q. Liu, R. Yu, J. Wang, N. B. Lin, X. Y. Liu, *Adv. Funct. Mater.* **2019**, 29.
[190] a) B. Yang, W. Zeng, Z. H. Peng, S. R. Liu, K. Chen, X. M. Tao, *Advanced Energy Materials* **2016**, 6; b) B. Yang, X. M. Tao, Z. H. Peng, *Nano Energy* **2019**, 57, 66; c) X. M. Tao, *Accounts Chem Res* **2019**, 52, 307; d) J. Song, B. Yang, W. Zeng, Z. H. Peng, S. P. Lin, J. Li, X. M. Tao, *Advanced Materials Technologies* **2018**, 3; e) S. Chen, X. M. Tao, W. Zeng, B. Yang, S. M. Shang, *Adv Energy Mater* **2017**, 7; f) J. L. Gong, B. G. Xu, X. M. Tao, *Acs Appl Mater Inter* **2017**, 9, 4988; g) F. R. Fan, Z. Q. Tian, Z. L. Wang, *Nano Energy* **2012**, 1, 328; h) T. Huang, C. Wang, H. Yu, H. Z. Wang, Q. H. Zhang, M. F. Zhu, *Nano Energy* **2015**, 14, 226; i) Z. L. Wang, L. Lin, J. Chen, S. Niu, Y. Zi, *Triboelectric nanogenerators*, Springer, **2016**; j) Y. Zi, J. Wang, S. Wang, S. Li, Z. Wen, H. Guo, Z. L. Wang, *Nature communications* **2016**, 7, 1; k) S. R. Liu, W. Zheng, B. Yang, X. M. Tao, *Nano Energy* **2018**, 53, 383.
[191] R. Riemer, A. Shapiro, *Journal of neuroengineering and rehabilitation* **2011**, 8, 22.
[192] a) Y. F. Hu, Z. J. Zheng, *Nano Energy* **2019**, 56, 16; b) L. S. Zhang, S. P. Lin, T. Hua, B. L. Huang, S. R. Liu, X. M. Tao, *Advanced Energy Materials* **2018**, 8; c) W. Zeng, X. M. Tao, S. P. Lin, C. Lee, D. L. Shi, K. H. Lam, B. L. Huang, Q. M. Wang, Y. Zhao, *Nano Energy*

2018, 54, 163; d) L.-S. Zhang, B. Yang, S.-P. Lin, T. Hua, X.-M. Tao, *Nano Energy* **2020**, 105117.
[193] a) W. Zeng, L. Shu, Q. Li, S. Chen, F. Wang, X. M. Tao, *Adv Mater* **2014**, 26, 5310; b) X. Pu, W. X. Song, M. M. Liu, C. W. Sun, C. H. Du, C. Y. Jiang, X. Huang, D. C. Zou, W. G. Hu, Z. L. Wang, *Adv Energy Mater* **2016**, 6, 1601048.
[194] K. Dong, X. Peng, Z. L. Wang, *Adv Mater* **2020**, 32, 1902549.
[195] J. L. Gong, B. G. Xu, X. Y. Guan, Y. J. Chen, S. Y. Li, J. Feng, *Nano Energy* **2019**, 58, 365.
[196] P. Fraga-Lamas, T. M. Fernández-Caramés, Ó. Blanco-Novoa, M. A. Vilar-Montesinos, *Ieee Access* **2018**, 6, 13358.
[197] a) G. Kim, K. Lee, Y. Kim, S. Park, I. Hong, K. Bong, H.-J. Yoo, *Ieee J Solid-St Circ* **2014**, 50, 113; b) I. Hong, K. Bong, D. Shin, S. Park, K. Lee, Y. Kim, H.-J. Yoo, presented at 2015 IEEE International Solid-State Circuits Conference-(ISSCC) Digest of Technical Papers **2015**.
[198] S. Chen, X. Tao, S. Shang, Springer SBM **2015**.
[199] a) X. Pu, W. G. Hu, Z. L. Wang, *Small* **2018**, 14, 1702817; b) L. Liu, W. Tang, C. Deng, B. Chen, K. Han, W. Zhong, Z. L. Wang, *Nano Research* **2018**, 11, 3972; c) J. Wang, W. Ding, L. Pan, C. Wu, H. Yu, L. Yang, R. Liao, Z. L. Wang, *ACS nano* **2018**, 12, 3954; d) K. Dai, X. Wang, F. Yi, C. Jiang, R. Li, Z. You, *Nano Energy* **2018**, 45, 84; e) X. He, Y. L. Zi, H. Y. Guo, H. W. Zheng, Y. Xi, C. S. Wu, J. Wang, W. Zhang, C. H. Lu, Z. L. Wang, *Advanced Functional Materials* **2017**, 27.
[200] W. Seung, M. K. Gupta, K. Y. Lee, K. S. Shin, J. H. Lee, T. Y. Kim, S. Kim, J. Lin, J. H. Kim, S. W. Kim, *Acs Nano* **2015**, 9, 3501.
[201] Q. He, Y. F. Wu, Z. P. Feng, W. J. Fan, Z. W. Lin, C. C. Sun, Z. H. Zhou, K. Y. Meng, W. Z. Wu, J. Yang, *J Mater Chem A* **2019**, 7, 26804.
[202] F. Wen, H. Wang, T. He, Q. Shi, Z. Sun, M. Zhu, Z. Zhang, Z. Cao, Y. Dai, T. Zhang, *Nano Energy* **2020**, 67, 104266.
[203] X.-m. Tao, Vol. 575, Nature Publishing Group, 2019, 453.
[204] Q. Huang, D. Wang, H. Hu, J. Shang, J. Chang, C. Xie, Y. Yang, X. Lepró, R. H. Baughman, Z. Zheng, *Advanced Functional Materials* **2020**, 1910541.
[205] J. Sun, Y. Huang, C. Fu, Y. Huang, M. Zhu, X. Tao, C. Zhi, H. Hu, *J. Mater. Chem. A* **2016**, 4, 14877.
[206] Y. Wang, S. Su, L. Cai, B. Qiu, N. Wang, J. Xiong, C. Yang, X. Tao, Y. Chai, *Adv Energy Mater* **2019**, 9, 1900037.
[207] S. S. Kwak, H. J. Yoon, S. W. Kim, *Advanced Functional Materials* **2019**, 29.
[208] A. C. Siegel, S. T. Phillips, M. D. Dickey, N. S. Lu, Z. G. Suo, G. M. Whitesides, *Adv. Funct. Mater.* **2010**, 20, 28.
[209] T. Sekitani, U. Zschieschang, H. Klauk, T. Someya, *Nat Mater* **2010**, 9, 1015.
[210] a) Y. H. Jung, T.-H. Chang, H. Zhang, C. Yao, Q. Zheng, V. W. Yang, H. Mi, M. Kim, S. J. Cho, D.-W. Park, *Nat Commun* **2015**, 6, 7170; b) S. Wang, T. Chinnasamy, M. A. Lifson, F. Inci, U. Demirci, *Trends in biotechnology* **2016**, 34, 909; c) K. G. Shah, P. Yager, *Anal Chem* **2017**, 89, 12023.
[211] R. Guo, X. Wang, H. Chang, W. Yu, S. Liang, W. Rao, J. Liu, *Adv. Eng. Mater.* **2018**, 20, 1800054.
[212] a) F. L. Li, Q. Qin, Y. L. Zhou, Y. Z. Wu, W. H. Xue, S. Gao, J. Shang, Y. W. Liu, R. W. Li, *Advanced Materials Technologies* **2018**, 3; b) R. Guo, J. Tang, S. Dong, J. Lin, H. Wang, J. Liu, W. Rao, *Advanced Materials Technologies* **2018**, 1800265.
[213] Y.-L. Park, C. Majidi, R. Kramer, P. Bérard, R. J. Wood, *J Micromech Microeng* **2010**, 20, 125029.
[214] R. Guo, L. Sheng, H. Gong, J. Liu, *Science China Technological Sciences* **2018**, 61, 516.
[215] S. W. Jin, J. Park, S. Y. Hong, H. Park, Y. R. Jeong, J. Park, S.-S. Lee, J. S. Ha, *Sci. Rep.* **2015**, 5, 11695.

[216] M. Hambsch, K. Reuter, M. Stanel, G. Schmidt, H. Kempa, U. Fügmann, U. Hahn, A. Hübler, *Materials Science and Engineering: B* **2010**, 170, 93.
[217] A. C. Hübler, F. Doetz, H. Kempa, H. E. Katz, M. Bartzsch, N. Brandt, I. Hennig, U. Fügmann, S. Vaidyanathan, J. Granstrom, *Organic Electronics* **2007**, 8, 480.
[218] Y. Wang, H. Guo, J. J. Chen, E. Sowade, Y. Wang, K. Liang, K. Marcus, R. R. Baumann, Z. S. Feng, *Acs Applied Materials & Interfaces* **2016**, 8, 26112.
[219] H. Yan, Z. Chen, Y. Zheng, C. Newman, J. R. Quinn, F. Dötz, M. Kastler, A. Facchetti, *Nature* **2009**, 457, 679.
[220] J. E. Thompson, *J Chem-Ny* **2017**, DOI: 10.1155/2017/4909327.
[221] J. H. Park, M. J. Park, J. S. Lee, *Nanoscale* **2017**, 9, 555.
[222] Y. Zhang, L. Zhang, K. Cui, S. Ge, X. Cheng, M. Yan, J. Yu, H. Liu, *Adv Mater* **2018**, 30, 1801588.
[223] X. Liao, Z. Zhang, Q. Liao, Q. Liang, Y. Ou, M. Xu, M. Li, G. Zhang, Y. Zhang, *Nanoscale* **2016**, 8, 13025.
[224] Q. Li, X. M. Tao, presented at Proceedings of the Royal Society of London A: Mathematical, Physical and Engineering Sciences **2014**.
[225] Q. Li, H. Chen, Z. Y. Ran, L. N. Zhang, R. F. Xiang, X. Wang, X. M. Tao, X. Ding, *Smart Mater Struct* **2018**, 27.
[226] T. Agcayazi, K. Chatterjee, A. Bozkurt, T. K. Ghosh, *Advanced Materials Technologies* **2018**, 3.
[227] M. Carbone, C. Freschi, S. Mascioli, V. Ferrari, M. Ferrari, in *Augmented Reality, Virtual Reality, and Computer Graphics, Pt Ii*, Vol. 9769 (Eds: L. T. DePaolis, A. Mongelli) **2016**, p. 92.
[228] Z. Yang, Y. Pang, X. L. Han, Y. F. Yang, J. Ling, M. Q. Jian, Y. Y. Zhang, Y. Yang, T. L. Ren, *ACS Nano* **2018**, 12, 9134.
[229] W. Zhou, S. Yao, H. Wang, Q. Du, Y. Ma, Y. Zhu, *ACS Nano* **2020**, 14, 5798.
[230] a) D. Freeman, S. Reeve, A. Robinson, A. Ehlers, D. Clark, B. Spanlang, M. Slater, *Psychological medicine* **2017**, 47, 2393; b) G. Guazzaroni, *Virtual and Augmented Reality in Mental Health Treatment*, IGI Global, **2018**; c) S. Casas, C. Portalés, L. Vera, J. V. Riera, in *Virtual and Augmented Reality in Mental Health Treatment*, IGI Global **2019**, p. 95; d) V. Lush, C. Buckingham, S. Wileman, S. Edwards, U. Bernardet, presented at 2019 5th Experiment International Conference (exp. at'19) **2019**; e) T. M. Fleming, L. Bavin, K. Stasiak, E. Hermansson-Webb, S. N. Merry, C. Cheek, M. Lucassen, H. M. Lau, B. Pollmuller, S. Hetrick, *Frontiers in psychiatry* **2017**, 7, 215.
[231] a) L. Bozgeyikli, A. Raij, S. Katkoori, R. Alqasemi, *Ieee T Learn Technol* **2018**, 11, 133; b) P. Mesa-Gresa, H. Gil-Gomez, J. A. Lozano-Quilis, J. A. Gil-Gomez, *Sensors-Basel* **2018**, 18; c) D. Johnston, H. Egermann, G. Kearney, *Appl Sci-Basel* **2020**, 10; d) I. Valori, R. Bayramova, P. E. McKenna-Plumley, T. Farroni, *Brain Sci* **2020**, 10.
[232] E. Ambron, A. Miller, K. J. Kuchenbecker, L. J. Buxbaum, H. B. Coslett, *Frontiers in Neurology* **2018**, 9.
[233] a) C. Botella, J. Breton-Lopez, S. Quero, R. Banos, A. Garcia-Palacios, *Behav Ther* **2010**, 41, 401; b) M. C. Juan, M. Alcaniz, C. Monserrat, C. Botella, R. M. Banos, B. Guerrero, *Ieee Comput Graph* **2005**, 25, 31; c) M. C. Juan, C. Botella, R. Banos, M. Alcaniz, D. Joele, C. van der Mast, *Cyberpsychol Behav* **2006**, 9, 684.
[234] a) M. Krijn, P. M. G. Emmelkamp, R. P. Olafsson, R. Biemond, *Clinical Psychology Review* **2004**, 24, 259; b) C. B. Pull, *Curr Opin Psychiatr* **2005**, 18, 7; c) T. D. Parsons, A. A. Rizzo, *J Behav Ther Exp Psy* **2008**, 39, 250; d) K. Meyerbroker, P. M. G. Emmelkamp, *Depression and Anxiety* **2010**, 27, 933; e) R. A. McCann, C. M. Armstrong, N. A. Skopp, A. Edwards-Stewart, D. J. Smolenski, J. D. June, M. Metzger-Abamukong, G. M. Reger, *J Anxiety Disord* **2014**, 28, 625; f) C. F. Tsai, S. C. Yeh, Y. Y. Huang, Z. Y. Wu, J. J. Cui, L. R. Zheng, *J Healthc Eng* **2018**, 2018; g) A. A. Benbow, P. L. Anderson, *J Anxiety Disord*

2019, 61, 18; h) D. Boeldt, E. McMahon, M. McFaul, W. Greenleaf, *Frontiers in Psychiatry* **2019**, 10; i) E. Carl, A. T. Stein, A. Levihn-Coon, J. R. Pogue, B. Rothbaum, P. Emmelkamp, G. J. G. Asmundson, P. Carlbring, M. B. Powers, *J Anxiety Disord* **2019**, 61, 27; j) A. Ghita, O. Hernandez-Serrano, J. Ruiz, M. Monras, L. Ortega, S. Mondon, L. Teixidor, A. Gual, B. Porras-Garcia, M. Ferrer-Garcia, J. Gutierrez-Maldonado, *Ann Rev Cybertherapy* **2019**, 17, 77; k) E. K. Yuen, E. M. Goetter, M. J. Stasio, P. Ash, B. Mansour, E. McNally, M. Sanchez, E. Hobar, S. Forte, K. Zulaica, J. Watkins, *J Context Behav Sci* **2019**, 12, 47; l) O. D. Kothgassner, A. Felnhofer, *Neuropsychiatrie* **2020**, DOI: 10.1007/s40211-020-00349-7.

[235] a) E. Bekele, D. Bian, J. Peterman, S. Park, N. Sarkar, *Ieee T Neur Sys Reh* **2017**, 25, 739; b) B. Horan, P. Harvey, A. Atkins, M. Narasimhan, T. Patterson, K. Richard, *Neuropsychopharmacol* **2019**, 44, 341; c) T. Skoneczny, E. Tyburski, J. Kucharska-Mazur, J. Samochowiec, *Eur Psychiat* **2019**, 56, S515.

[236] a) G. Riva, M. Bacchetta, M. Baruffi, E. Molinari, *Cyberpsychol Behav* **2001**, 4, 511; b) G. Riva, M. Bacchetta, M. Baruffi, E. Molinari, *Ieee Transactions on Information Technology in Biomedicine* **2002**, 6, 224.

[237] E. Richard, V. Billaudeau, P. Richard, G. Gaudin, *2007 Virtual Rehabilitation* **2007**, 100.

[238] a) A. Mirelman, I. Maidan, T. Herman, J. E. Deutsch, N. Giladi, J. M. Hausdorff, *The Journals of Gerontology: Series A* **2011**, 66, 234; b) F. A. dos Santos Mendes, J. E. Pompeu, A. M. Lobo, K. G. da Silva, T. de Paula Oliveira, A. P. Zomignani, M. E. P. Piemonte, *Physiotherapy* **2012**, 98, 217; c) A. Mirelman, I. Maidan, J. E. Deutsch, *Movement Disord* **2013**, 28, 1597; d) G. Abbruzzese, R. Marchese, L. Avanzino, E. Pelosin, *Parkinsonism Relat D* **2016**, 22, S60; e) B. Bluett, E. Bayram, I. Litvan, *Parkinsonism Relat D* **2019**, 61, 26; f) I. Cikajlo, K. P. Potisk, *Journal of Neuroengineering and Rehabilitation* **2019**, 16.

[239] D. W. Man, B. Ganesan, C. C. Yip, C. O. Lee, S. Y. Tsang, P. W. Yu, J. G. Young, D. H. Shum, *Neuropsychological rehabilitation* **2018**, 28, 1197.

[240] L. C. Chang, C. Y. Wang, P. Yu, *Int J Geriatr Psych* **2014**, 29, 1312.

[241] P. K.-T. Li, K. M. Chow, M. W. Van de Luijtgaarden, D. W. Johnson, K. J. Jager, R. Mehrotra, S. Naicker, R. Pecoits-Filho, X. Q. Yu, N. Lameire, *Nature Reviews Nephrology* **2017**, 13, 90.

[242] J. Park, J. Yim, *Tohoku J Exp Med* **2016**, 238, 1.

[243] C. S. Lin, M. Y. Jeng, T. M. Yeh, *Int J Env Res Pub He* **2018**, 15.

[244] a) A. J. Blake, K. Morgan, M. J. Bendall, H. Dallosso, S. B. J. Ebrahim, T. H. D. Arie, P. H. Fentem, E. J. Bassey, *Age Ageing* **1988**, 17, 365; b) B. H. Wood, J. A. Bilclough, A. Bowron, R. W. Walker, *J Neurol Neurosur Ps* **2002**, 72, 721; c) A. Mirelman, L. Rochester, M. Reelick, F. Nieuwhof, E. Pelosin, G. Abbruzzese, K. Dockx, A. Nieuwboer, J. M. Hausdorff, *Bmc Neurology* **2013**, 13; d) A. Talamo, M. Camilli, L. Di Lucchio, S. Ventura, *Universal Access Inf* **2017**, 16, 739.

[245] a) J. M. Hausdorff, G. Yogev, S. Springer, E. S. Simon, N. Giladi, *Experimental Brain Research* **2005**, 164, 541; b) J. M. Hausdorff, G. Yogev, *Journal of the American Geriatrics Society* **2006**, 54, 865; c) J. M. Hausdorff, M. E. Nelson, D. Kaliton, J. E. Layne, M. J. Bernstein, A. Nuernberger, M. A. F. Singh, *J Appl Physiol* **2001**, 90, 2117; d) T. Herman, A. Mirelman, N. Giladi, A. Schweiger, J. M. Hausdorff, *J Gerontol a-Biol* **2010**, 65, 1086; e) K. S. van Schooten, E. Freiberger, M. Sillevis Smitt, V. Keppner, C. Sieber, S. R. Lord, K. Delbaere, *Physical Therapy* **2019**, 99, 989.

[246] a) X. Shen, I. S. K. Wong-Yu, M. K. Y. Mak, *Neurorehabilitation and Neural Repair* **2016**, 30, 512; b) C. L. Chung, M. K. Y. Mak, *Brain Stimulation* **2016**, 9, 475; c) I. S. Wong-Yu, M. K. Mak, *Parkinsonism Relat D* **2015**, 21, 615; d) I. S. Wong-Yu, M. K. Mak, *Arch Phys Med Rehab* **2015**, 96, 2103; e) X. Shen, M. K. Mak, *Neurorehabilitation and neural repair* **2015**, 29, 103; f) X. Shen, M. K. Mak, *Neurorehabilitation and neural repair*

2014, 28, 524; g) M. Mak, M. Hallett, *Clinical Neurophysiology* **2013**, 124, 545; h) I. S. Wong-Yu, M. K. Mak, *Am J Phys Med Rehab* **2019**, 98, 239.
[247] M. K. Mak, I. S. Wong-Yu, X. Shen, C. L. Chung, *Nat Rev Neurol* **2017**, 13, 689.
[248] X. Tao, *Handbook of smart textiles*, Springer, **2015**.
[249] L. Wang, X. Fu, J. He, X. Shi, T. Chen, P. Chen, B. Wang, H. Peng, *Adv Mater* **2020**, 32, e1901971.
[250] H. L. Sun, K. Dai, W. Zhai, Y. J. Zhou, J. W. Li, G. Q. Zheng, B. Li, C. T. Liu, C. Y. Shen, *Acs Applied Materials & Interfaces* **2019**, 11, 36052.
[251] J. Lee, H. Sul, Y. Jung, H. Kim, S. Han, J. Choi, J. Shin, D. Kim, J. Jung, S. Hong, *Adv. Funct. Mater.* **2020**, 30, 2003328.
[252] Z. T. Zhang, L. Y. Cui, X. Shi, X. C. R. Tian, D. P. Wang, C. N. Gu, E. Chen, X. L. Cheng, Y. F. Xu, Y. J. Hu, J. Y. Zhang, L. Zhou, H. H. Fong, P. B. Ma, G. M. Jiang, X. M. Sun, B. Zhang, H. S. Peng, *Adv Mater* **2018**, 30.
[253] Y. Tsukada, M. Tokita, H. Murata, Y. Hirasawa, K. Yodogawa, Y. Iwasaki, K. Asai, W. Shimizu, N. Kasai, H. Nakashima, S. Tsukada, *Heart and Vessels* **2019**, 34, 1203.
[254] E. Lee, G. Cho, *Smart Mater Struct* **2019**, 28.
[255] R. Castrillon, J. J. Perez, H. Andrade-Caicedo, *Biomed Eng Online* **2018**, 17.
[256] X. An, G. K. Stylios, *Materials* **2018**, 11.
[257] A. Achilli, D. Pani, A. Bonfiglio, Ieee, in *2017 Computing in Cardiology*, Vol. 44 **2017**.
[258] D. Pani, A. Dessi, J. F. Saenz-Cogollo, G. Barabino, B. Fraboni, A. Bonfiglio, *Ieee T Bio-Med Eng* **2016**, 63, 540.
[259] Y. Noh, J. R. Bales, B. A. Reyes, J. Molignano, A. L. Clement, G. D. Pins, J. P. Florian, K. H. Chon, *Ann. Biomed. Eng.* **2016**, 44, 2464.
[260] R. H. Wu, L. Y. Ma, A. B. Patil, C. Hou, Z. H. Meng, Y. F. Zhang, X. Y. Liu, W. D. Yu, *Text. Res. J.* **2019**, 89, 5144.
[261] K. Kim, M. Jung, S. Jeon, J. Bae, *Smart Mater Struct* **2019**, 28.
[262] Z. Q. Zhou, Y. Li, J. Cheng, S. Y. Chen, R. Hu, X. W. Yan, X. Q. Liao, C. M. Xu, J. S. Yu, L. Li, *J. Mater. Chem. C* **2018**, 6, 13120.
[263] L. Zhang, H. Q. Li, X. J. Lai, T. Y. Gao, J. Yang, X. R. Zeng, *Acs Applied Materials & Interfaces* **2018**, 10, 41784.
[264] S. Wang, H. M. Ning, N. Hu, Y. L. Liu, F. Liu, R. Zou, K. Y. Huang, X. P. Wu, S. Y. Weng, Alamusi, *Advanced Materials Interfaces* **2020**, 7.
[265] C. S. Luo, B. Tian, Q. Liu, Y. Feng, W. Wu, *Advanced Materials Technologies* **2020**, 5.
[266] L. Gan, A. B. Geng, Y. Wu, L. J. Wang, X. Y. Fang, L. J. Xu, C. T. Mei, *Polymers* **2020**, 12.
[267] K. R. Reddy, S. Gandla, D. Gupta, *Advanced Materials Interfaces* **2019**, 6.
[268] S. W. Lu, S. Wang, G. D. Wang, J. C. Ma, X. Q. Wang, H. L. Tang, X. D. Yang, *Sensor Actuat a-Phys* **2019**, 295, 200.
[269] X. A. Huang, Q. Wang, S. Y. Zang, J. X. Wan, G. Yang, Y. Q. Huang, X. M. Ren, *IEEE Sensors J.* **2019**, 19, 9504.
[270] M. X. Bai, Y. J. Zhai, F. Liu, Y. A. Wang, S. D. Luo, *Sci. Rep.* **2019**, 9.
[271] C. C. Vu, J. Kim, *Sensor Actuat a-Phys* **2018**, 283, 263.
[272] H. Lee, M. J. Glasper, X. D. Li, J. A. Nychka, J. Batcheller, H. J. Chung, Y. Chen, *J Mater Sci* **2018**, 53, 9026.
[273] J. Ko, S. Jee, J. H. Lee, S. H. Kim, *Sensor Actuat a-Phys* **2018**, 274, 50.
[274] S. J. Kim, W. Song, Y. Yi, B. K. Min, S. Mondal, K. S. An, C. G. Choi, *Acs Applied Materials & Interfaces* **2018**, 10, 3921.
[275] Y. Huang, L. Gao, Y. N. Zhao, X. H. Guo, C. X. Liu, P. Liu, *J. Appl. Polym. Sci.* **2017**, 134.
[276] J. Eom, R. Jaisutti, H. Lee, W. Lee, J.-S. Heo, J.-Y. Lee, S. K. Park, Y.-H. Kim, *ACS Applied Materials & Interfaces* **2017**, 9, 10190.
[277] X. D. Wu, Y. Y. Han, X. X. Zhang, C. H. Lu, *Acs Applied Materials & Interfaces* **2016**, 8, 9936.

[278] Z. F. Wang, Y. Huang, J. F. Sun, Y. Huang, H. Hu, R. J. Jiang, W. M. Gai, G. M. Li, C. Y. Zhi, *Acs Applied Materials & Interfaces* **2016**, 8, 24837.
[279] S. Chen, Z. Lou, D. Chen, K. Jiang, G. Shen, *Advanced Materials Technologies* **2016**, 1, 1600136.
[280] K. Suzuki, K. Yataka, Y. Okumiya, S. Sakakibara, K. Sako, H. Mimura, Y. Inoue, *Acs Sensors* **2016**, 1, 817.

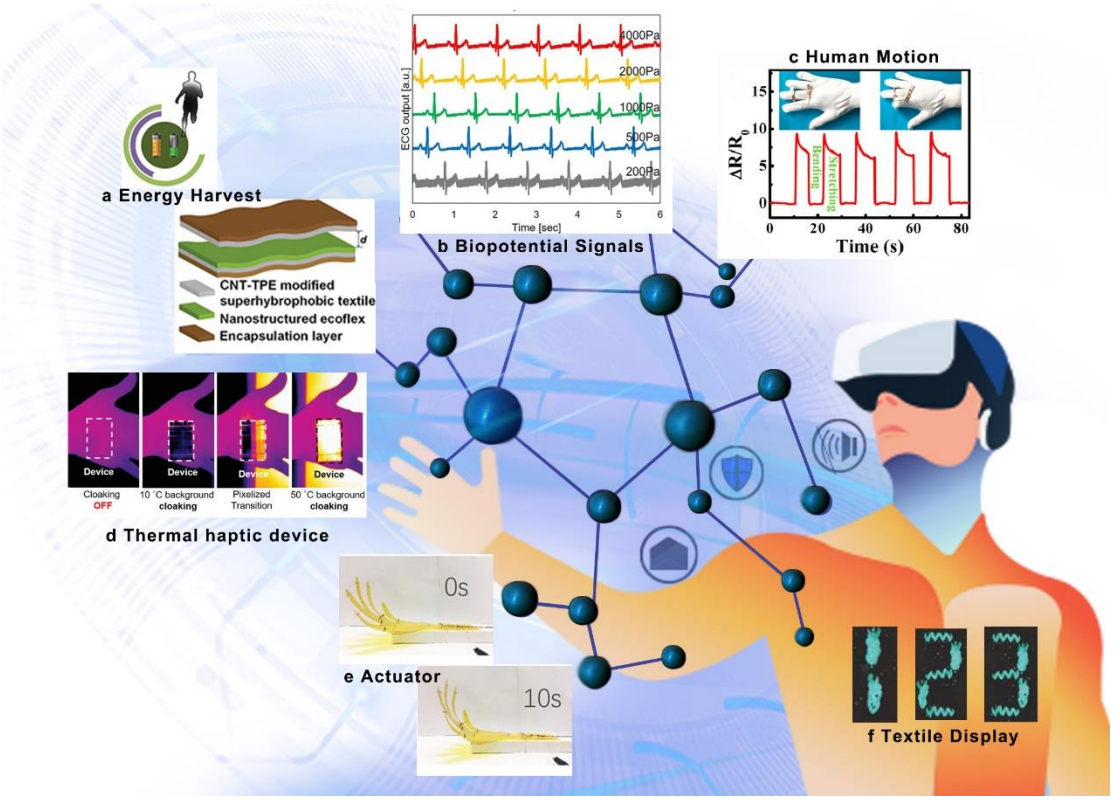

Figure 1 (a) Diagram of textile TENG. Reproduced with permission.[115] Copyright 2020, WILEY. (b) ECG signals. Reproduced with permission.[89] Copyright 2019, Springer Nature. (c) Resistance change of finger bending. Reproduced with permission.[250] Copyright 2019, ACS Publications. (d) Place thermal haptic device on the hand at cooling/heating model. Reproduced with permission.[251] Copyright 2020, WILEY. (e) Robotic hand driven by actuator. Reproduced with permission.[100] Copyright 2020, WILEY. (f) Textile display number. Reproduced with permission.[252] Copyright 2018.

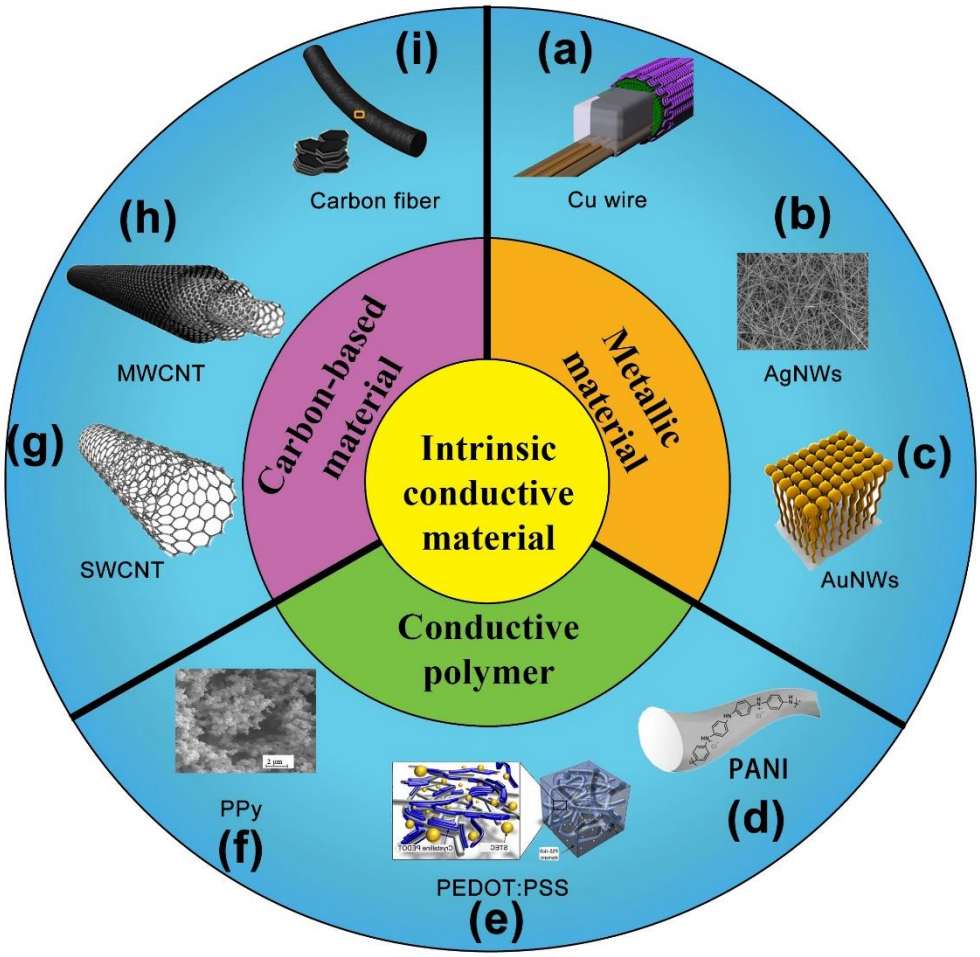

Figure 2 Intrinsic conductive material (a) Schematic of an electronic yarn with a copper wire and an electronic component. Reproduced with permission.[12] Copyright 2019, Springer. (b) SEM image of an AgNW film. Reproduced with permission.[17] Copyright 2012, WILEY. (c) Schematic illustration of AuNW. Reproduced with permission.[19] Copyright 2020, WILEY. (d) Conducting PANI fiber. Reproduced with permission.[22] Copyright 2016, WILEY. (e) PEPOT: PSS film with STEC enhancers. Reproduced with permission.[24] Copyright 2017, AAAS. (f) SEM image of PPy. Reproduced with permission.[27] Copyright 2018, ELSEVIER. (g) Structures of SWCNT, (h) Structures of MWCNT, (g) and (h) reproduced with permission.[29] Copyright 2017, ELSEVIER. (i) Carbon fiber. Reproduced with permission.[31] Copyright 2018, ELSEVIER.

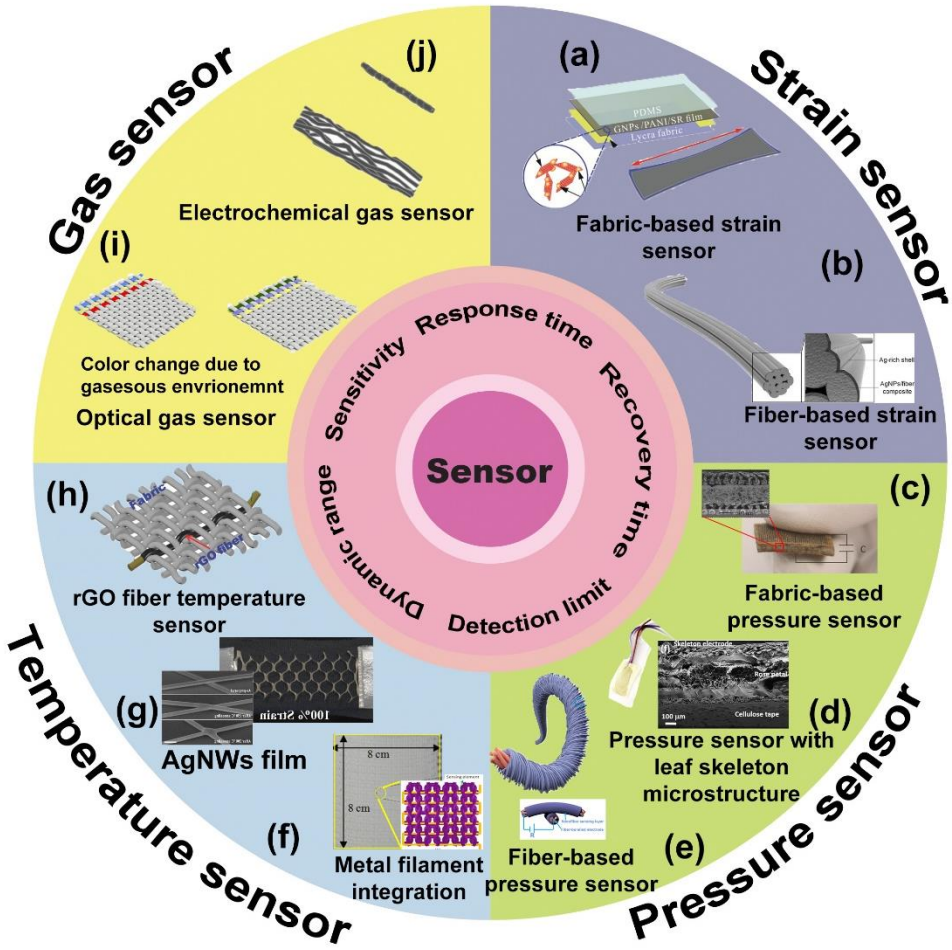

Figure 3 Textile sensors (a) Fabric-based strain senor. Reproduced with permission.[50] Copyright 2017, Wiley Periodicals. (b) Fiber-based strain sensor. Reproduced with permission.[52] Copyright 2018, ACS Publications. (c) Fabric-based pressure sensor. Reproduced with permission.[55] Copyright 2017, WILEY. (d) Microstructure of a pressure sensor. Reproduced with permission.[56] Copyright 2020, WILEY. (e) Fiber-based pressure sensor. Reproduced with permission.[57] Copyright 2020, ELSEVIER. (f) Temperature sensor with metal filament integration. Reproduced with permission.[63] Copyright 2013, MDPI. (g) AgNW film temperature sensor. Reproduced with permission.[64] Copyright 2019, ACS Publications. (h) rGO fiber temperature sensor. Reproduced with permission.[66] Copyright 2018, WILEY. (i) Optical gas sensor. Reproduced with permission.[68] Copyright 2019, Springer Nature. (j) Electrochemical gas sensor. Reproduced with permission.[69] Copyright 2017, ELSEVIER.

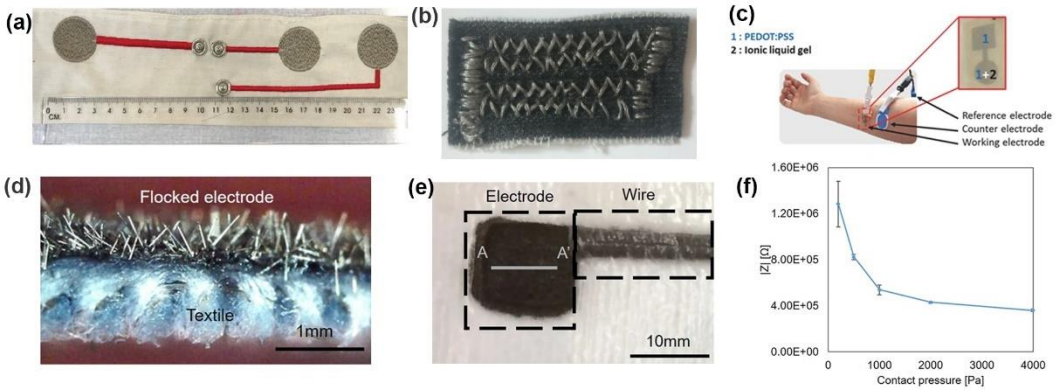

Figure 4 Textile electrodes (a) Image of electrodes with silver yarn. Reproduced with permission.[81] Copyright 2019, IEEE. (b) Image of electrodes with stainless steel yarn. Reproduced with permission.[75] Copyright 2020, University Stefan cel Mare Suceava. (c) Image of electrodes for impedance measurements. Reproduced with permission.[83] Copyright 2017, WILEY. (d) Cross-section of flocked electrode, (e) Image of electrodes and wires on a fabric, (f) Impedance vs contact pressure at 100 Hz, (d−f) Reproduced with permission.[89] Copyright 2019, Springer Nature.

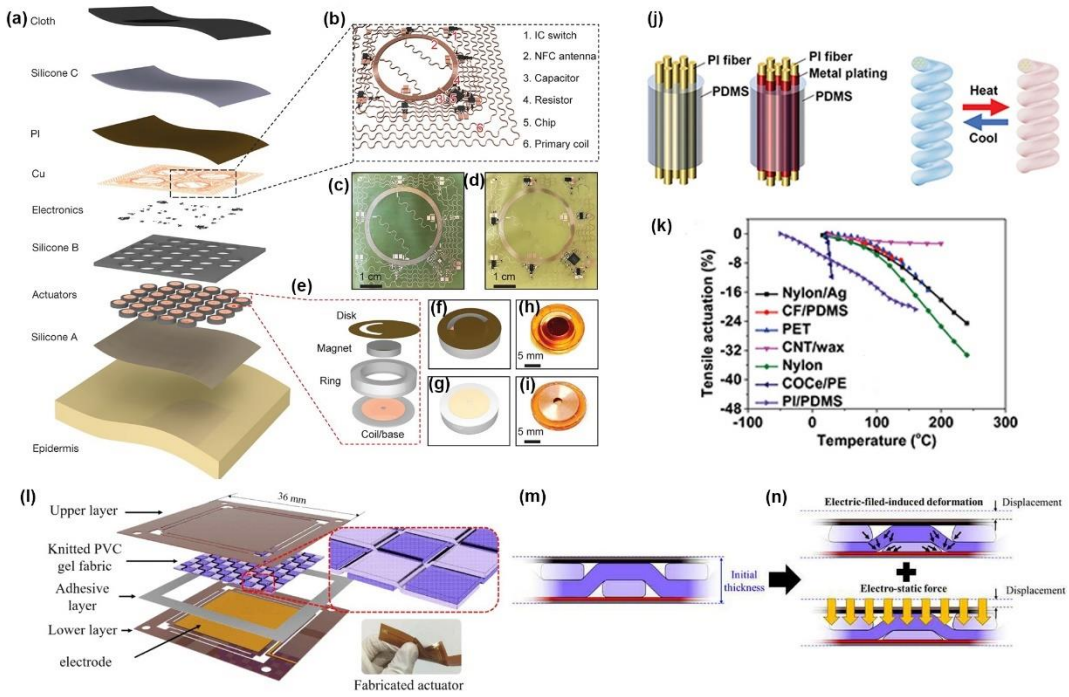

Figure 5 Textile haptic devices (a–i) Epidermal VR system architecture, (a) Haptic device—enlarged schematic with 32 independent control actuators, (b) NFC circuit and electronics schematic with six main components, (c) and (d) NFC coil optical image (c) before and (d) after the electronic component integration, (e) Actuator—enlarged schematic, (f) and (g) Actuator—schematic viewed from (f) top and (g) bottom, (h) and (i) Actuator—optical image viewed from (h) top and (i) bottom, (a–i) Reproduced with permission.[8] Copyright 2019, Nature Publishing Group. (j) Structure and components of thermally/electrothermally actuator, (k) Comparison of isotonic behavior among various fiber-based coiled linear actuators, (j–k) Reproduced with permission.[100] Copyright 2020, WILEY. (l) Textile haptic actuator with PVC knitted fabrics, (m) Actuator—initial state, (n) Actuator—working state with applied voltage. Reproduced with permission.[99] Copyright 2020, IEEE.

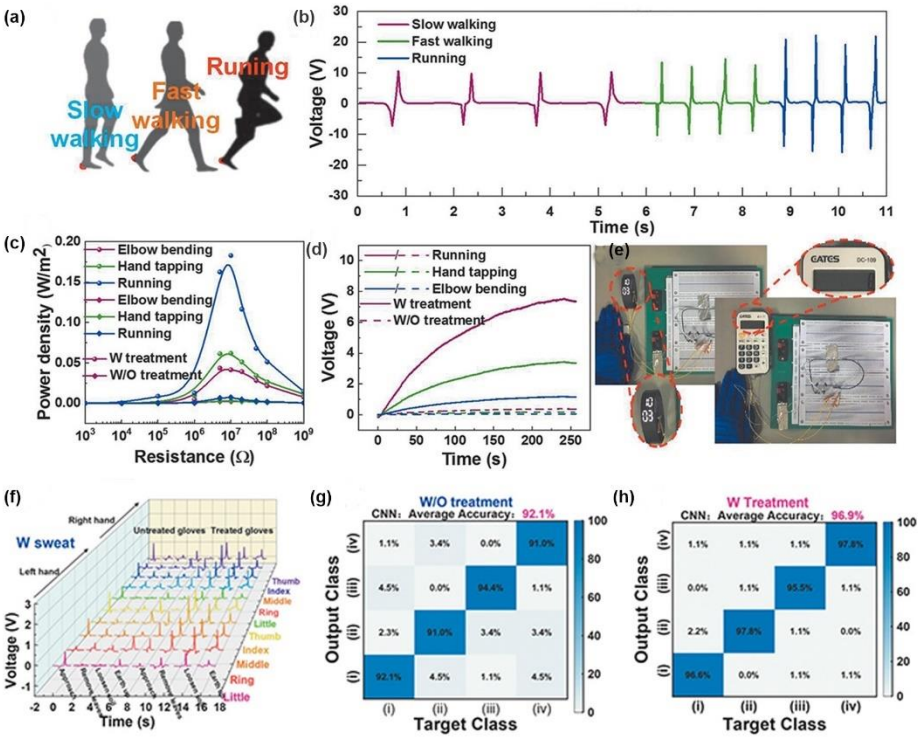

Figure 6 Self-powered textile devices for gesture recognition (a) Energy harvesting during walking and running, (b) Voltage curves of walking and running, (c) Output power with elbow bending, hand tapping, and running, (d) Charging curves of human motion, (e) Image of driving an electronic watch, (f) Signal patterns of gloves in a sweat environment, (g) and (h) Machine learning recognition accuracy of untreated and treated glove at a sweat climate (a−h) Reproduced with permission.[115] Copyright 2020, WILEY.

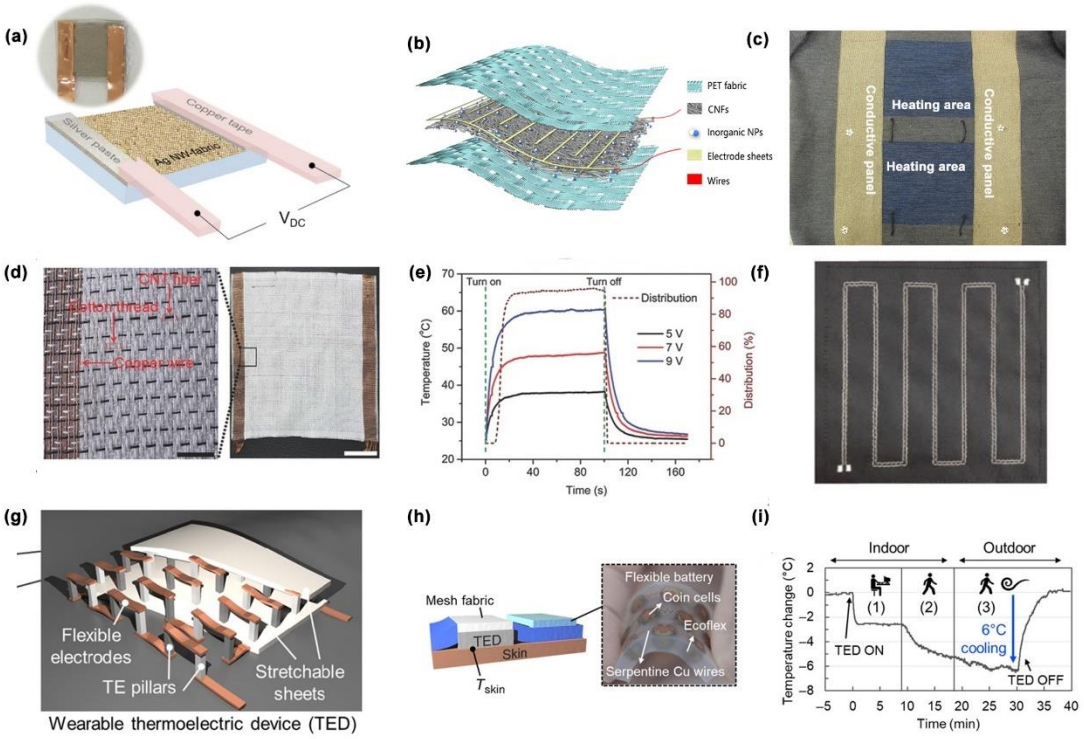

Figure 7 Microclimate device (a) Resistive heating textile with two electrodes. Reproduced with permission.[121] Copyright 2018, Springer Nature. (b) Composite heating fabric. Reproduced with permission.[123] Copyright 2020, ACS Publications. (c) Knitted heating fabric. Reproduced with permission.[124c] Copyright 2017, The Hong Kong Polytechnic University. (d) Woven heating textile, (e) Curves of temperature vs time and distribution vs time of the heating textile, (d) and (e) Reproduced with permission.[126] Copyright 2018, WILEY. (f) Embroidered heating textile. Reproduced with permission.[118] Copyright 2016, SAGE. (g) Schematic illustration of wearable TED, (h) Diagram of TED armband integrated with battery box (image in the dotted box), (i) Skin temperature controlled by TED cooling at sitting, walking indoors, and waling outdoors. (g–i) Reproduced with permission.[129b] Copyright 2019, WILEY.

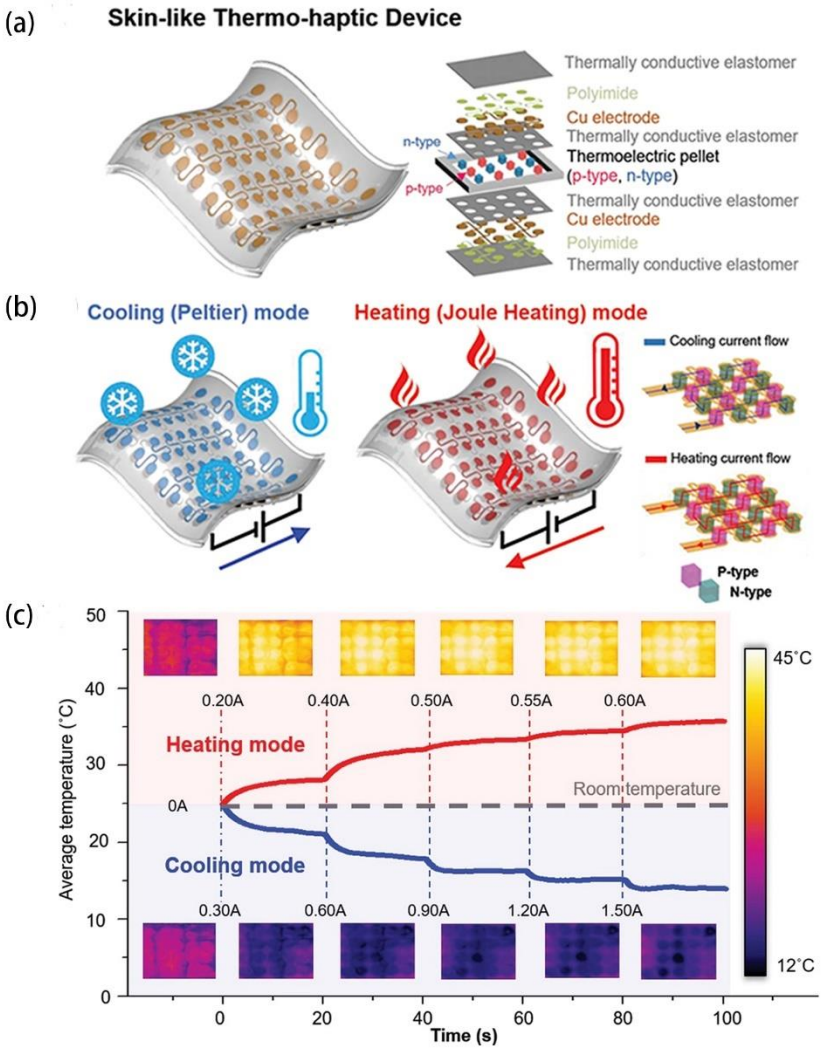

Figure 8 Skin-like thermo haptic device (a) Enlarged view and diagram of thermo haptic device, (b) Schematic of bio-functional (heating and cooling) device, (c) Temperature change and corresponding infrared camera images at two modes (heating and cooling). Reproduced with permission.[119] Copyright 2020, WILEY.

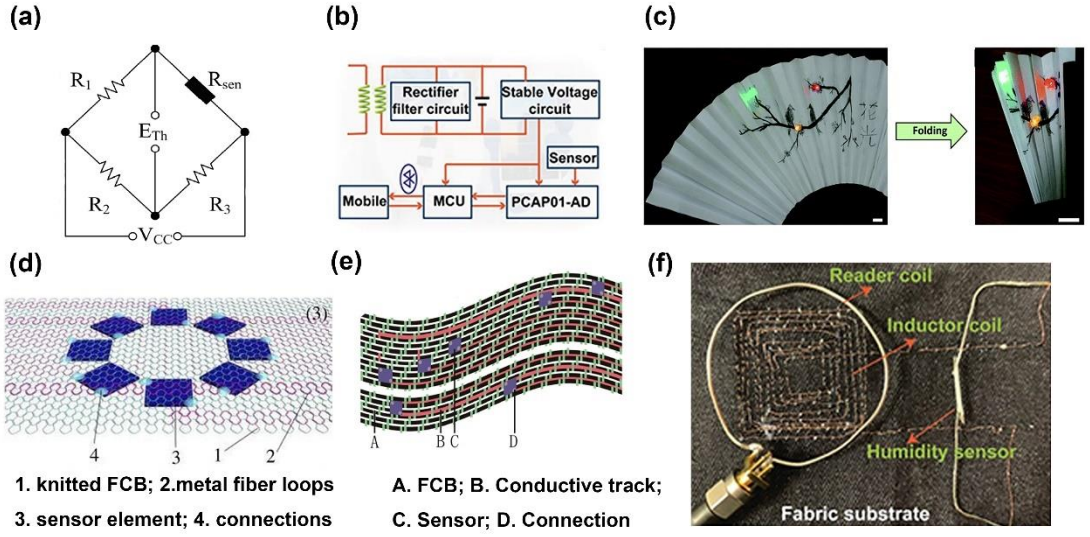

Figure 9 Electric interface and circuit board (a) Signal conditioning component: a single element bridge. Reproduced with permission.[188] Copyright 2012, The Hong Kong Polytechnic University. (b) Signal amplification and processing circuit. Reproduced with permission.[189] Copyright 2019, WILEY. (c) Paper circuits for LED on a handheld folding fan under unfolded and folded state. Reproduced with permission.[221] Copyright 2017, The Royal Society of Chemistry. (d) Knitted FCB. Reproduced with permission.[224] Copyright 2014, Royal Society Publishing. (e) Woven FCB. Reproduced with permission.[225] Copyright 2018, IOP Publishing. (f) Embroidery circuit board. Reproduced with permission.[189] Copyright 2019, WILEY.

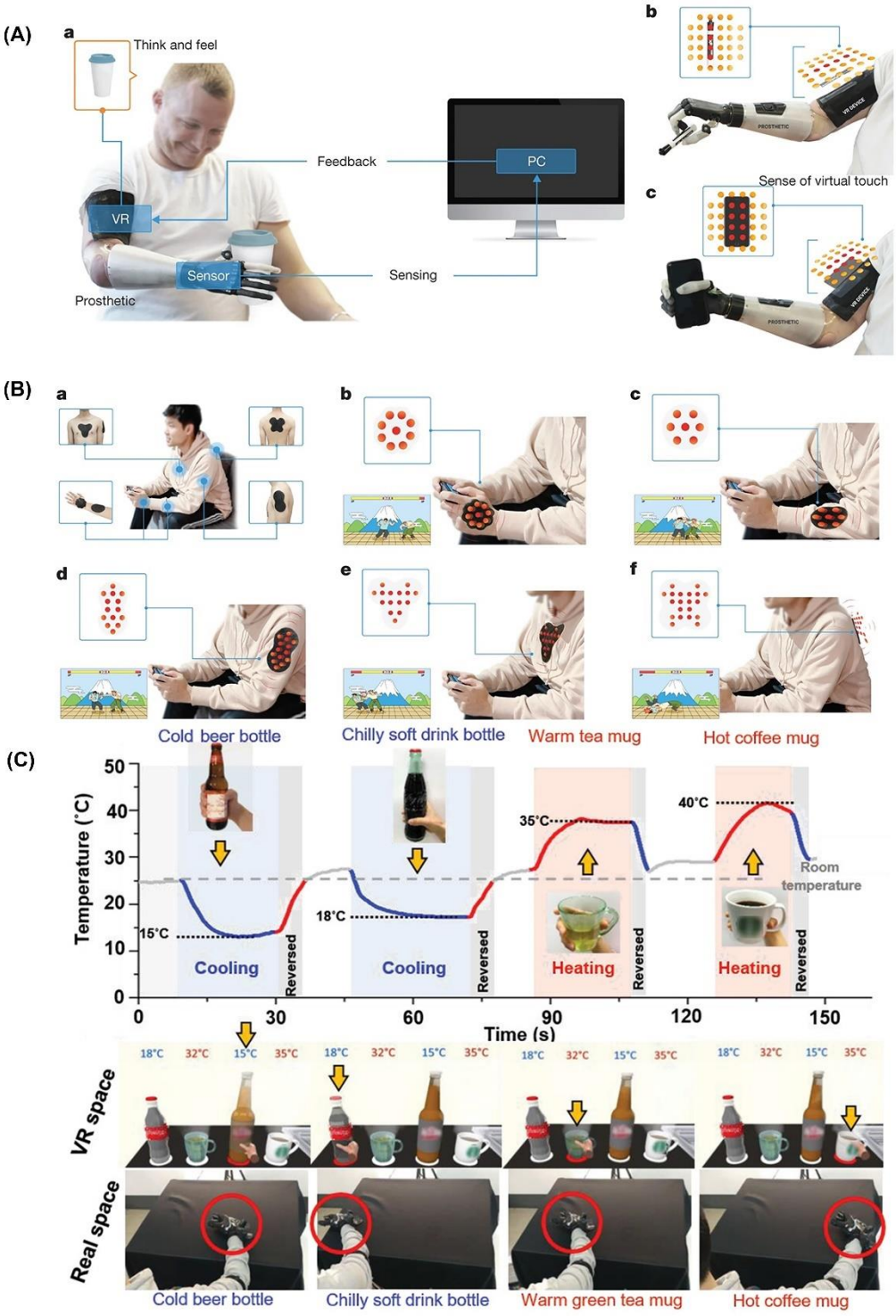

Figure 10 Applications of textile devices in VR/AR system (A) Prosthetics application: (a) a user with a lower-arm amputation puts on a prosthetic arm with an epidermal VR device and a robotic hand on the upper arm, (b) and (c) the device generates haptic sensation patterns ('think and feel') reproducing the shape features of an object ('feedback') grasped from the robotic hand ('sensing'), (B) Gaming application: (a) a user puts on epidermal VR devices on various body parts, (b−f) placement of VR devices, i.e., (b) hand, (c) elbow, (d) arm, (e) chest, and (f) back, (A) and (B) Reproduced with permission.[8] (A) and (B) Copyright 2019, Nature Publishing Group. (C) Regenerating virtual temperature changes based on virtual scenarios of contacting

objects with different temperatures. Reproduced with permission.[119] Copyright 2020, WILEY.

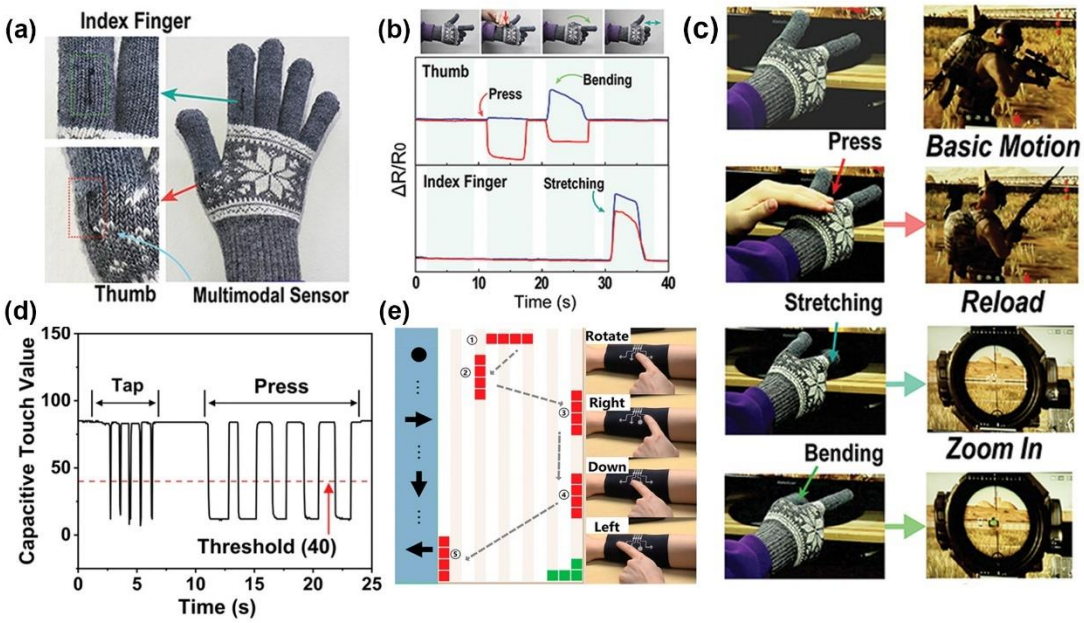

Figure 11 Posture and gait tracking devices (a) Image of multimodal fiber-type sensor integrated in glove for virtual interface control, (b) Measurements of sensor with response to different external stimuli, (c) Photo and virtual images of the smart glove applied in gaming. Reproduced with permission.[110] Copyright 2019, WILEY (d) Capacitive touch values of sensor, (e) Capacitive touch sensor applied in playing games, (d) and (e) Reproduced with permission.[229] Copyright 2020, ACS Publications.

Table 1. Performance of textile-based surface bio-potential electrodes

No.	Signal	Materials	Preparation method	Geometric size (mm)	Skin contact impedance	Sheet resistance /Resistance[#]	SNR (dB)	Bandwidth (Hz)	Year
1 [78a]	ECG	Knitted fabric coated with PEDOT:PSS	Dip coating	-	-	120 Ω	21.76	-	2020
2 [74]	ECG	silver electrode, fabric coated with copper and nickel	Layer by layer	30 × 25	360 kΩ to 10 kΩ (< 1 M Ω/cm^2)	-	11.83	20−1000	2020
3 [82]	ECG	Silver thread sewed on fabric	Sewing	30 × 30	-	0.3 Ω [#]	-	2000	2020
4 [253]	ECG	Nano fibers coated with PEPOT-PSS	Coating	40 × 40 40 × 80 100 × 28	-	1.26 kΩ	-	0.01−1000	2019
5 [89]	ECG	Ag plated fiber on textile	Electrostatic flocking	10 × 10	500 kΩ	30.6 Ω [#]		1−10000	2019
6 [77]	EEG	Conductive fabric and foam	Layer by layer	29 × 18 × 4 (L×W×H)	46.82 kΩcm^2	-	-	0.1−1000	2019
7 [78b]	EMG	Textile printed with PEPDO: PSS	Screen printing	φ24 φ10	~700 kΩ ~900 kΩ	390 Ω/sq 410 Ω/sq	-	10−1000	2019
8 [254]	ECG	PU coated SWCNT and AgNW	Dip coating	30 × 30	~420 kΩ	18.4 Ω/cm [#]	-	50−1000	2019
9 [81]	ECG	Silver thread on fabric	Embroidering	φ30	-	5.48 Ω	39.4	0−100	2019
10 [79]	ECG	Bacterial cellulose fiber coated polyaniline	Dip coating	φ16	51 kΩ	-	-	1−100	2018
11 [76]	ECG	Yarn coated with silver or metal	Knitting	100 × 100	1–5 MΩ/cm^2	0.2 Ω/cm [#]	25-33	-	2018
12 [255]	ECG	Fabric coated PEDPT: PSS	Coated	20 × 20	1 MΩ@1 Hz	-	-	0.1−10000	2018
13 [256]	ECG	Silver plated nylon	Knitted	15 × 15	300Ω@20 Hz	-	-	20−20000	2018
14 [83]	ECG	PEDOT: PSS coated fabric	Inkjet printing	10 × 10	0.08 MΩ@1 Hz	0.5 kΩ [#]	-	0.1−1000	2017
15 [257]	ECG	PEDOT: PSS coated fabric	Screen printing	20 × 20	80 kΩ	-	-	0−500	2017
16 [258]	ECG	PEDOT: PSS coated textile	Coating	30 × 30	40 kΩ@20 Hz	-	-	20−500	2016

17 [259]	ECG	Carbon black and PDMS	Mixed	20 (diameter) × 2 (thickness)	100 kΩ@10 Hz	-	-	0−1000	2016
18 [84]	ECG	PEDOT: PSS on textiles	Direct patterning	10 × 10	100 kΩ@10 Hz	-		1−1000	2015

Table 2. Performance of textile-based pressure sensors for gesture and gait recognition

No.	Mechanism	Materials	Preparation method	Range (kPa)	Sensitivity (kPa^{-1})	Measured parameter	Analysis method	Number of sensors	Year
1 [115]	Triboelectric	CNT coated textile	Spray coating	-	-	Finger bending degree	Machine learning	1 per finger	2020
2 [114a]	Triboelectric	Conductive fabric, PVDF/Ag NW NFM and PDMS	Layering	0−3 3−32	1.67 V 0.2 V	Elbow, knee and ankle bending	Amplitude	1 per unit	2020
3 [111]	Triboelectric	Nylon and PTFE filament	Twisting and weaving	1.95−3.13 3.20−4.61	1.33 V 0.32 V	Hand, elbow, knee and underarm bending, etc.	Amplitude	1 per unit	2020
4 [109c]	Resistive	AgNW and latex foam	Dip-coating	-	-	Pressure of fingertip	Amplitude	1 per finger	2019
5 [116]	Resistive	Force sensitive film and	Lacer cutting and screen printing	-	-	Hand gesture	Machine learning	548 per hand	2019
6 [114b]	Triboelectric	PEDOT: PSS coated textile	Dip-coating	-	-	Finger bending degree	Amplitude	1 per finger	2019
7 [202]	Triboelectric	Conductive textile	Layering			Car control	Amplitude	8 per device	2019
8 [260]	Capacitive	Conductive fabric and elastomer Ecoflex	Megnetron sputtering	0−16	0.035	Finger bending, touching and knocking	Amplitude	1 per unit	2019
9 [113]	Capacitive	Textile plated with metal and rubber	Plating	-	-	Gait pattern analysis	Software	10 per insole	2019
10 [261]	Resistive	CNT coated Aytextile	Dip-coating	0.2−50	-	Pulse pressure and jugular vein measurement, finger bending, cheek bulging, etc.	Amplitude	1 per unit	2019
11 [262]	Resistive	AgNW-coated cotton and silver printed on cotton	Coating and screen printing	0−30	2.46×10^4- 5.65×10^5	Finger and wrist bending, finger motion	Amplitude	1 per unit	2018
12 [263]	Resistive	GO coated fabric	Coating and overlay	0−8 30−200	8.37 0.028	Wrist pulse, visual angle of eye, voice recognition, finger and leg movement	Amplitude	1 per unit	2018
13 [114c]	Resistive	CNT coated cotton fabric	Coating	-	-	Finger bending	Amplitude	1 per finger	2018
14 [55]	Capacitive	Conductive textile and microporous dielectric silicon layer	lamination	1−100		Finger grasp force	Amplitude	1 per finger	2018

Table 3. Performance of textile-based strain sensors for gesture and gait recognition

No.	Mechanism	Materials	Preparation method	GF	Stretchability (%)	Measured parameter	Analysis method	Number of sensors	Year
1 [109a]	Resistive	Carbon coated textile	Dip-coating	62.9	30	Finger joint, chest movement, wrist bending, elbow joint, etc.	Amplitude	1 per unit	2020
2 [264]	Resistive	Graphite coated silk textile	Vacuum filtration	124.5	10	Finger bending, eye blinking, wrist flexion, etc.	Amplitude	1 per unit	2020
3 [109b]	Triboelectric	Conductive fabric and PU	Spin-coating	-	3	Elbow movement, toe contact movement, palm-flapping exercise, etc.	Amplitude	1 per unit	2020
4 [265]	Resistive	AgNW printed textile	Screen printing	216	120	Finger, wrist and elbow bending, walking	Amplitude	1 per unit	2020
5 [266]	Resistive	MWCNTs/Ag/PLA Nanofibrous Membrane	Electrospinning and dip-coating	-	5	Finger, inner elbow and knee bending, forehead movement	Amplitude	1 per unit	2029
6 [267]	Resistive	RGO and polyester knitted fabric	Chemical reduction	30	1	Index finger, wrist joint, knee joint, cheek, etc.	Amplitude	1 per unit	2019
7 [110]	Resistive	Conductive fiber	Dip-coating and pressure-assisted imprinting	1021	200	Finger bending degree	Amplitude	1 per finger	2019
8 [267]	Resistive	RGO and polyester knitted fabric	Chemical reduction	30 34 5	1 20 20−50	Index finger, wrist joint, knee joint, cheek, etc.	Amplitude	1 per unit	2019
9 [250]	Resistive	CNTs/PU yarns	Dip-coating	5	20−50	Index finger and wrist bending, knee joint and eye movement, etc.	Amplitude	1 per unit	2019

10 [110]	Resistive	Conductive fiber	Dip-coating and pressure-assisted imprinting	1021	200	Finger bending degree	Amplitude	1 per finger	2019
11 [268]	Resistive	Graphene film and fabric	Pressing	47.6	19	Finger, wrist, knee and elbow bending, etc.	Amplitude	1 per unit	2019
12 [269]	Resistive	RGO coated fiber	Coating	1.25	20	Finger bending and gesture recognition	Software	10 per glove	2019
13 [270]	Resistive	GO coated yarn	Coating and reducing	12.06	50	Finger bending, lower leg and elbow movement	Amplitude	1 per unit	2019
14 [228]	Resistive	GO coated fabric	Coating and reducing	-26 -1.7	8 15	Finger, wrist, knee and elbow bending, facial expression, mouth motion, etc.	Amplitude	1 per unit	2018
15 [117a]	Resistive	SWCNT coated fabric	Coating	4.1−8.5	50	Human motion such as walking, running, sprinting and jumping	Machine learning	1 per leg	2018
16 [271]	Resistive	SWCNT coated fabric	Dip coating	3.5−8.5	50	Human motion such as sitting, standing, limping, etc.	Fuzzy inference system	1 per leg	2018
17 [272]	Resistive	GO coated fabric	Dip coating	6.33 18.24	6.67 40.6	Finger bending	Amplitude	1 per finger	2018
18 [273]	Resistive	MWCNT coated fabric	Vacuum-filtration and screen-printing	-	20	Finger bending	Amplitude	1 per finger	2018
19 [274]	Resistive	rGO/SWCNTs coated fabric	Dip coating	4−6.1 2−2.9 0.8−1.2	3.3−5.5 5.5−9.3 9.3−11.6	Finger bending and grabbing, wrist motion	Amplitude	2 per finger	2018
20 [275]	Resistive	GNPs/PANI/SR coated fabric	Spin-coating	67.3	40	Finger bending	Amplitude	1 per finger	2017
21 [276]	Resistive	PEDOT coated fiber	Dip coating	0.1/0.7 0.6/0.2	20 50 70	Leg movement, finger bending	Amplitude	1 per unit	2017

				0.2/0.2					
22 [164]	Capacitive	Conductive fabric and silicone layer	Layering	1.23	100	Finger gesture	Amplitude	2 per unit	2017
23 [277]	Resistive	CPC@PU yarn	Dip coating	38.9	0.1	Speech recognition, wrist signal, forehead and philtrum expression	Amplitude	1 per unit	2016
24 [278]	Resistive	PU/cotton/CNT yarn	Dip coating	2.15 0.65	0−25 25−240	Finger movements and elbow motions	Amplitude	1 per unit	2016
25 [279]	Resistive	P(VDF-TrFE) based conductive fiber	Electrospinning and dip coating	5.32	25	Finger bending, wrist pulse and speaking recognition	Amplitude	1 per unit	2016
26 [280]	Resistive	CNT and textile	Impregnating CNT sheet with resin	10	200	Finger bending degree	Amplitude	2 per finger	2016